Catalysis Science & Technology

PERSPECTIVE

View Article Online
View Journal | View Issue

Cite this: *Catal. Sci. Technol.*, 2015, 5, 1991

Solar thermal catalytic reforming of natural gas: a review on chemistry, catalysis and system design

David S. A. Simakov,[a] Mark M. Wright,[ab] Shakeel Ahmed,[c] Esmail M. A. Mokheimer[d] and Yuriy Román-Leshkov*[a]

Received 13th October 2014,
Accepted 6th January 2015

DOI: 10.1039/c4cy01333f

www.rsc.org/catalysis

Solar radiation is an abundant and environmentally benign energy source. However, its capture and effective utilization is one of the most difficult challenges faced by modern science. An effective way to capture solar energy is to convert it to chemical energy using concentrated solar power and thermochemical conversion routes, such as methane reforming. Methane, the main component of natural gas, is poised to become a leading feedstock in the near term, partly due to recent developments in shale gas extraction. Solar-to-chemical energy conversion can be achieved by reforming methane into synthesis gas, a mixture of carbon monoxide and hydrogen, in a single, highly endothermic catalytic process when reacted with steam or carbon dioxide. This review highlights different aspects of solar thermal reforming of methane, including thermodynamics, challenges related to catalyst activity and stability and reactor design. Equilibrium limitations are discussed in detail with respect to solar thermal reforming. Recent developments in methane reforming catalysis are critically reviewed in a broad scope, addressing catalyst deactivation drawbacks and focusing on alternative catalysts. The potential of the low-temperature solar methane steam reforming and the related technological challenges are discussed, including catalyst requirements. Future directions are also outlined.

[a] *Department of Chemical Engineering, Massachusetts Institute of Technology, Cambridge, MA 02139, USA. E-mail: yroman@mit.edu; Tel: (+1) 617 258 0431*
[b] *Department of Mechanical Engineering, Iowa State University, Ames, IA 50011, USA*
[c] *Center for Refining and Petrochemicals, Research Institute, King Fahd University of Petroleum and Minerals, Dhahran 31261, Kingdom of Saudi Arabia*
[d] *Department of Mechanical Engineering, King Fahd University of Petroleum & Minerals, Dhahran 31261, Kingdom of Saudi Arabia*

1. Introduction

Solar radiation is an abundant energy source, which is, however, difficult to capture and utilize in an efficient way. Solar energy can be used for direct electricity generation using photovoltaic cells.[1] Currently, a significant fraction of solar installations are based on photovoltaics, with a continuously

David S. A. Simakov

David Simakov received his Ph. D. in Chemical Engineering from the Technion – Israel Institute of Technology working on design of catalytic membrane reactors for hydrogen generation from methane. He also worked in industry on development of a new generation of fuel cells. After the completion of his Ph.D., he worked on mathematical modeling of biological pattern formation, participating in a joint project between the Technion and Princeton University. He then moved to Harvard University, where he studied oscillatory behavior of catalytic chemical systems. His current research at MIT focuses on catalyst and reactor design for solar thermal conversion of natural gas.

Mark M. Wright

Dr. Mark M. Wright is an Assistant Professor in Mechanical Engineering at Iowa State University. His research interests are in the development and evaluation of biomass conversion technologies using techno-economic analysis, life-cycle assessment, and uncertainty quantification.

growing market that already exceeds 100 GW of global installed capacity. However, the limiting energy conversion efficiencies and relatively high cost of this technology preclude its growth unless substantial subsidies are provided. Solar thermal energy conversion, wherein radiant solar energy is concentrated, absorbed by a receiver and transferred as thermal energy to a working fluid, is an alternative option that already features commercial installations totaling several GWs globally.[2–6]

Conventional concentrated solar power (CSP) technology is based on focusing sunlight with a reflecting surface (*e.g.*, a mirror) to heat a fluid flowing through a collector (Fig. 1). There are four types of collectors: parabolic troughs (PT), Fresnel reflectors (FR), solar towers (ST) and solar dishes (SD),[5] with PTs being the most commercially mature technology (representing more than 90% of the currently installed CSP capacity). The first three types of collectors are mostly used for centralized electricity generation, while solar dishes are more suitable for distributed generation. The heated fluid (*e.g.*, pressurized steam) can be used to supply (solar) heat for end-use applications or to generate electricity through steam turbines. Other heat transfer fluids, such as synthetic oils or molten salts, which have higher heat capacities than steam, can be also used for electricity generation through downstream steam generation *via* heat exchange. An important advantage of the CSP technology is that it can be easily integrated into existing fossil fuel-based power plants that use gas and steam turbines. In this case, the heat produced by the fossil fuel combustion can be partially substituted by

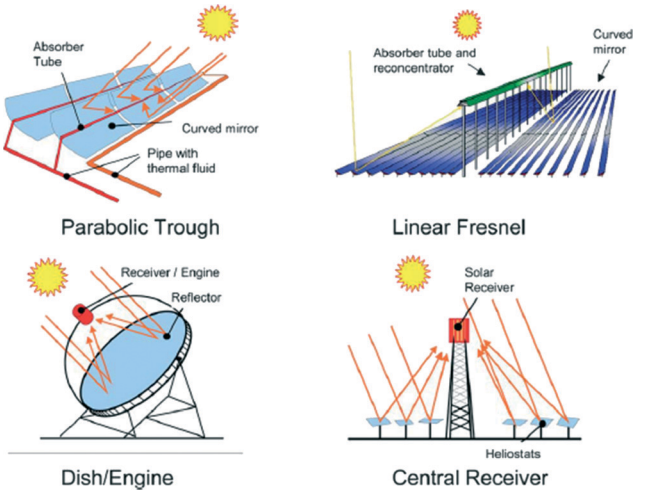

Fig. 1 Four types of solar collectors: parabolic trough (PT), linear Fresnel reflector (FR), solar dish (SD) and central receiver, also known as solar tower (ST). PT and FR are linear focus systems providing temperatures ranging from *ca.* 300–550 °C, while SD and ST are point focus concentrators providing temperatures above 850 °C. Reproduced from ref. 5.

Shakeel Ahmed

Dr. Shakeel Ahmed is Research Scientist at the Center for Refining and Petrochemicals, King Fahd University of Petroleum & Minerals, Dhahran, Saudi Arabia. He received PhD degree in Chemistry (catalysis) from KFUPM in 1995. His research interests are in the area of industrial catalysis for refining applications. He has authored over 130 papers in international journals and conference proceedings. He is also co-inventor of 32 patents related to catalysis for various energy and environmental applications. Currently he is developing a catalytic technology for hydrogen production from liquid hydrocarbon fuels for on-board as well as stationary power generation applications.

Esmail M. A. Mokheimer

Dr. Esmail M. A. Mokheimer is a professor of Mechanical Engineering at KFUPM. His research interests are in the area of computational and experimental fluid dynamics and heat transfer. He has published over 70 papers in reputable refereed international journals and conferences in this area. Dr. Mokheimer used to develop his own CFDHT codes. Recently, Dr. Mokheimer is focusing on Energy savings aspects as well as the use of renewable energy. Dr. Mokheimer is now leading more than one project on integrating Concentrated Solar Power Technologies with Conventional Power Plants with a focus on fuel reforming and fuel combustion technologies.

Yuriy Román-Leshkov

Prof. Román obtained his B.S. in Chemical Engineering at the University of Pennsylvania and completed his Ph.D. at the University of Wisconsin-Madison under the guidance of Prof. James Dumesic working on catalytic strategies to convert biomass-derived carbohydrates into platform chemicals. Before joining the department of Chemical Engineering at MIT, he completed a postdoc at Caltech, working with Prof. Mark E. Davis on zeolite synthesis. His research lies at the interface of heterogeneous catalysis and materials design, where a wide range of synthetic, spectroscopic, and reaction engineering tools are applied to study the chemical transformation of molecules on catalytic surfaces.

the heat from the CSP plant (originated from solar energy), reducing fossil fuel consumption, carbon dioxide emissions, and other types of pollution. Notably, large CSP plants can be equipped with heat storage systems that allow the supply of heat or electricity at night.

Recently, there has been a growing interest in using CSP for solar thermochemical synthesis.[5–8] In a CSP solar thermochemical process, concentrated solar radiation is used as a source of energy (in form of heat) to drive highly endothermic reactions. The product of such a process is commonly referred to as a "solar fuel", which contains a fraction of chemical energy that originated from solar energy. There are several solar thermochemical pathways which include splitting of water, reduction of carbon dioxide, gasification or cracking of fossil fuels (coal, oil, natural gas), biomass gasification and natural gas reforming.[5,6] Among these, solar thermal reforming of natural gas is probably the most promising, due to large resources of natural gas worldwide. The resulting solar fuel (hydrogen or syngas) can be used as a chemical feedstock or as a combustion fuel for electricity generation using gas turbines.[7]

The potential of natural gas is becoming increasingly important due to recent developments in horizontal drilling and hydraulic fracturing technology for the extraction of shale gas (natural gas trapped within shale formations). According to the U.S. Energy Information Administration (EIA), proven reserves of natural gas increased from 191 743 to 283 879 standard billion cubic feet in recent years. These discoveries have precipitated a decline in natural gas prices from a high of $13.07 per 1000 standard cubic feet ($462 m^{-3}) in 2008 to an average of $2.01 per 1000 standard cubic feet on April, 2012.[9] The fraction of natural gas supplied by shale gas is expected to increase significantly during the coming decades, providing security of energy supply, lowering prices for consumers, and reducing greenhouse gas emissions by replacing, for instance, coal.

The composition of natural gas varies between gas wells, but it is mostly composed of methane (CH_4, typically >90%) with small amounts of ethane, carbon dioxide and negligible quantities of longer-chained hydrocarbons and impurities. Conventionally, natural gas is converted to synthesis gas (syngas, a mixture of carbon monoxide and hydrogen) *via* the steam reforming process catalyzed by nickel-based catalysts. Hydrogen production from natural gas (the main source of hydrogen in chemical industry) also requires additional steps of water gas shift (WGS) and separation, most commonly by pressure swing adsorption (PSA). According to the United State Department of Energy, 95% of the hydrogen produced in the United States is made by natural gas reforming in large reforming facilities.

Methane steam reforming (MSR) is a highly endothermic, reversible process with methane conversion thermodynamically favored by high temperatures and low pressures (*vide infra*). The thermodynamic properties of the MSR reaction require temperatures well above 800 °C in order to obtain nearly complete methane conversions at elevated pressures required in industrial installations. In CSP systems, such high temperatures can be only achieved using solar towers and parabolic dishes. However, complete methane conversions are not necessary required for applications that involve electricity generation from solar-enriched natural gas using gas turbines.[7] This allows, in principle, the use of parabolic troughs that operate at temperatures below 600 °C (ref. 5) for upgrading natural gas. In addition to the thermodynamic equilibrium limitations, operating at these lower temperature regimes also has consequences for catalyst activity and stability (this topic is discussed in section 3).

An alternative process (with similar thermodynamic limitations) for syngas generation is methane dry reforming (MDR), wherein carbon dioxide (CO_2) is used as an oxidant instead of steam. In contrast to steam, CO_2 is not readily available and, despite an apparent potential of this approach for CO_2 sequestration, CO_2 separation, storage and supply are probably too costly to make this route economically feasible in the near future. There are other routes of methane conversion such as (commercialized) autothermal reforming and partial oxidation[10–13] and more exotic approaches in the very first stages of development such as catalytic aromatization of methane.[13,14] The main disadvantage of the autothermal reforming and partial oxidation is strong dilution of the reactive stream by nitrogen when air is used as a source of oxygen (using pure oxygen is disadvantageous from the economic point of view and for safety reasons).

In this work, we review different aspects of solar thermal reforming of methane. First, we analyze equilibrium constrains of methane steam and dry reforming, considering also water gas shift, in view of the application of this processes to thermochemical natural gas conversion using concentrated solar power. Next, the review focuses on recent developments in methane reforming catalysis (including Density Functional theory predictions, catalyst deactivation issues and alternative catalysts) and catalyst requirements for solar reforming. This is followed by a review of current reactor design solutions for solar reforming of methane. Future directions and recommendations are also presented.

2. Equilibrium limitations

2.1. Thermochemistry of methane reforming

MSR, eqn (1), or MDR, eqn (2), to form hydrogen (H_2) and carbon monoxide (CO), are highly endothermic, reversible reactions with the total increase in number of moles:[15–18]

$$\text{MSR: } CH_4 + H_2O \rightleftarrows CO + 3H_2 \quad \Delta H_{MSR} = +206.1 \text{ kJ mol}^{-1} \quad (1)$$

$$\text{MDR: } CH_4 + CO_2 \rightleftarrows 2CO + 2H_2 \quad \Delta H_{DSR} = +247.3 \text{ kJ mol}^{-1} \quad (2)$$

Although CH_4 conversion is thermodynamically favored at high temperature (temperatures of *ca.* 800–1000 °C are used in industry) and low pressure, industrial reformers have to be operated at elevated pressures ranging from 3 to 25 bar. The heat is typically supplied by burning a fraction of the natural

gas feed. Because of the high reaction enthalpies, heat inputs that are equivalent to a significant fraction of the feed energy value (25.7% and 30.8% for complete CH_4 conversion in MSR and MDR respectively, assuming a CH_4 heat of combustion of 802 kJ mol^{-1}) are required. Steam generation for MSR also consumes a large amount of energy (water heat of vaporization is 40.7 kJ mol^{-1}, implying *ca.* 15% of the CH_4 energy value for steam-to-carbon ratio of 3). In principle, the heat required for the endothermic reaction and steam generation can be provided by solar energy using CSP, saving a very significant fraction of otherwise burned natural gas, while also reducing CO_2 emissions. Evidently, CSP installations will require additional capital cost investments and can be only effectively used in the regions that have high solar fluxes throughout the year. Developing novel catalysts and reformer designs is critical for the use of CSP in CH_4 reforming (these topics are discussed in sections 3 and 4).

Other important reactions that can take place during the reforming process are the water gas shift (WGS) reaction, eqn (3), and carbon deposition (coking), eqn (4)–(6).[17–22]

$$\text{WGS: } CO + H_2O \rightleftarrows CO_2 + H_2 \quad \Delta H_{WGS} = -41.2 \text{ kJ mol}^{-1} \tag{3}$$

$$\text{MC: } CH_4 \rightleftarrows C + 2H_2 \quad \Delta H_{MC} = +74.8 \text{ kJ mol}^{-1} \tag{4}$$

$$\text{BR: } 2CO \rightleftarrows C + CO_2 \quad \Delta H_{BR} = -173.3 \text{ kJ mol}^{-1} \tag{5}$$

$$\text{RG: } CO + H_2 \rightleftarrows C + H_2O \quad \Delta H_{RG} = -131.3 \text{ kJ mol}^{-1} \tag{6}$$

The exothermic WGS reaction, which is carried out in separate downstream units in industrial installations, is used to increase H_2 yield from MSR (for H_2 production). The WGS reaction is undesirable for the Fischer–Tropsch process that ideally requires H_2/CO ratios of *ca.* 2 (the stoichiometry dictates H_2/CO = 3 and 1 for MSR and MDR, respectively, eqn (1) and (2)). Coking, which is a major problem encountered with industrial catalysts based on nickel (Ni), can occur by either methane cracking (MC) or Boudouard reaction (BC), or reverse gasification (RG), eqn (4)–(6),[19,21,22] and can eventually lead to reformer clogging. Thermodynamically speaking, carbon formation is less favorable at low temperatures and high steam-to-carbon ratios, Fig. 2.[22]

Industrial reformers are typically fed with steam-to-carbon ratios close to 3, which are far away from the carbon formation boundary (Fig. 2), effectively preventing coking, but resulting in a less efficient operation due to the increased energy demand for excess steam generation. Handling large amount of excess steam is particularly undesirable for solar reforming installations which require significant capital cost investments. It is imperative therefore to develop novel catalytic systems that can withstand low steam-to-carbon ratios without severe deactivation and degradation due to carbon formation.

2.2. Methane reforming equilibrium

Since methane reforming is a reversible process, its implementation in solar thermal reforming applications will be limited by equilibrium, which can be derived from standard thermodynamic parameters.[23,24] In the absence of carbon deposition, extents of species in equilibrium are expressed in terms of CH_4 conversion in the combined MSR–WGS process (f_1 and f_2 are total conversion and conversion to CO respectively, n is number of moles and subscripts f and eq stand for feed and equilibrium):

$$f_1 = \frac{n_{CH_4,f} - n_{CH_4,eq}}{n_{CH_4,f}} \tag{7}$$

$$f_2 = \frac{n_{CO,eq}}{n_{CH_4,f}} \tag{8}$$

Extents of species at the equilibrium are defined now as functions of f_1 and f_2 (α is feed steam-to-carbon ratio):

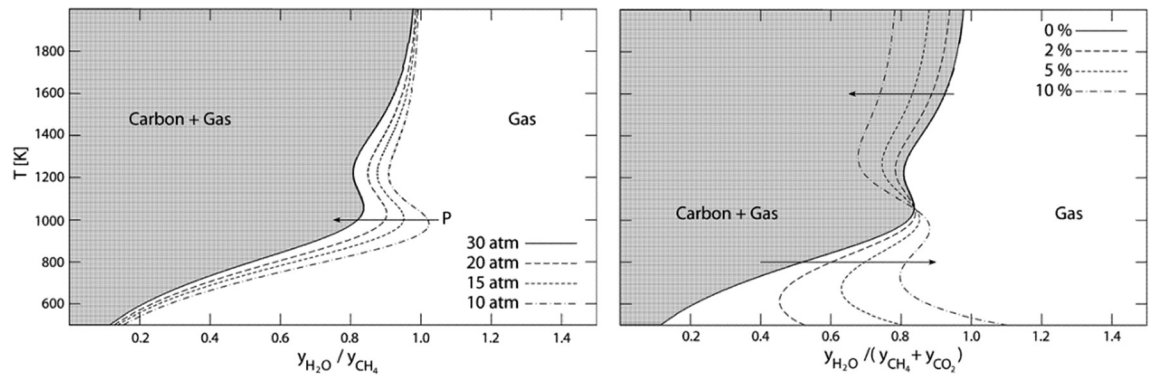

Fig. 2 Carbon formation equilibrium for a steam–methane system (left side) and for a steam–methane–carbon dioxide system (right side). The shaded area refers to the carbon formation zone at 30 atm. Limiting curves for different pressures (left side) and for different $CO_2/(CO_2 + CH_4)$ ratios (right side) are also shown. Reprinted with permission from ref. 22. Copyright (2014) AIDIC Servizi S.r.l.

$$\begin{aligned}\phi_{CH_4} &= 1 - f_1\\ \phi_{H_2O} &= \alpha - 2f_1 + f_2\\ \phi_{CO} &= f_2\\ \phi_{CO_2} &= f_1 - f_2\\ \phi_{H_2} &= 4f_1 - f_2\\ \alpha &= \frac{n_{H_2O,f}}{n_{CH_4,f}}\end{aligned} \quad (9)$$

Equilibrium partial pressures (p_i) are defined now in terms of species extent (y_i is molar fraction and P is total pressure):

$$p_i = y_i P = \frac{\phi_i}{\sum_i \phi_i} P \quad (10)$$

Eqn (10) is now substituted into the definitions of the MSR and WGS equilibrium constants:

$$K_{eq,MSR} = \frac{p_{CO} p_{H_2}^{\ 3}}{p_{CH_4} p_{H_2O}} \quad (11)$$

$$K_{eq,WGS} = \frac{p_{CO_2} p_{H_2}}{p_{CO} p_{H_2O}} \quad (12)$$

Rearrangement results in two nonlinear equations:

$$A_{eq,MSR} \exp\left(\frac{-E_{eq,MSR}}{R_g T}\right)\frac{1}{P^2} = \frac{f_2(4f_1 - f_2)^3}{(1-f_1)(\alpha - 2f_1 + f_2)(1 + \alpha + 2f_1)^2} \quad (13)$$

$$A_{eq,WGS} \exp\left(\frac{-E_{eq,WGS}}{R_g T}\right) = \frac{(f_1 - f_2)(4f_1 - f_2)}{f_2(\alpha - 2f_1 + f_2)} \quad (14)$$

Following the same approach, we can derive equilibrium for the combined MDR-RWGS (reverse water gas shift) process (f_3 is RWGS extent):

$$f_3 = \frac{n_{H_2O,eq}}{n_{CH_4,f}} \quad (15)$$

$$\begin{aligned}\phi_{CH_4} &= 1 - f_1\\ \phi_{H_2O} &= f_3\\ \phi_{CO} &= 2f_1 + f_3\\ \phi_{CO_2} &= 1 - f_1 - f_3\\ \phi_{H_2} &= 2f_1 - f_3\end{aligned} \quad (16)$$

$$K_{eq,MDR} = \frac{p_{CO}^{\ 2} p_{H_2}^{\ 2}}{p_{CH_4} p_{CO_2}} \quad (17)$$

$$A_{eq,MDR} \exp\left(\frac{-E_{eq,MDR}}{R_g T}\right)\frac{1}{P^2} = \frac{(2f_1 + f_3)^2 (2f_1 - f_3)^2}{(1-f_1)(1-f_1-f_3)(2+2f_3)^2} \quad (18)$$

$$A_{eq,WGS} \exp\left(\frac{-E_{eq,WGS}}{R_g T}\right) = \frac{(1-f_1-f_2)(2f_1 - f_2)}{(2f_1 + f_2) f_2} \quad (19)$$

Equilibrium conversions are calculated by solving numerically eqn (13) and (14) for f_1 and f_2 (for the MSR + WGS system) or eqn (18) and (19) for f_1 and f_3 (for the MDR + RWGS system); parameters (A_{eq} and E_{eq}) are listed in the literature.[20]

Fig. 3 shows the calculated equilibrium conversions in the parametric domain of pressure and temperature, which can be divided into three temperature regimes: low temperature (<600 °C), intermediate regime (600–900 °C) and high temperature regime (>900 °C). These regimes coincide with the temperature ranges obtainable by different types of solar concentrators (Fig. 1). Linear focus systems (FR and PT) cover the low temperature regime; point focus systems (SD and ST) typically provide intermediate temperatures, while high temperature regime is exclusively achievable by central receivers

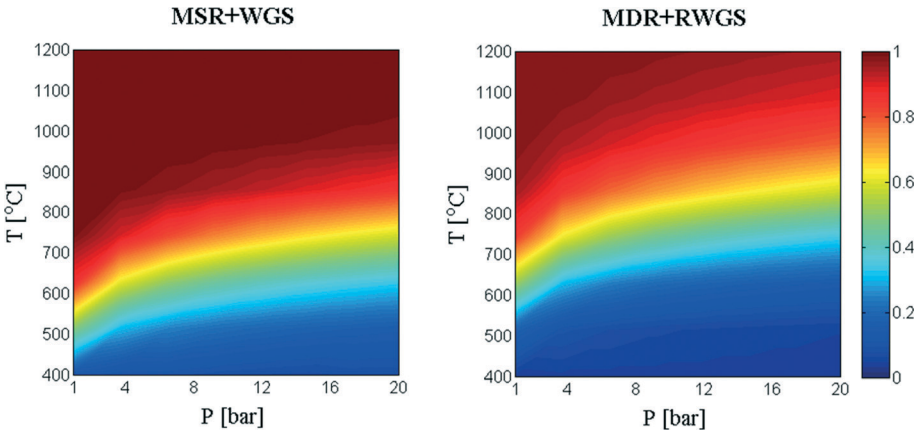

Fig. 3 Equilibrium CH_4 conversion for the combined MSR and WGS (left side) and MDR and RWGS (right side) processes is shown in the parametric domain of temperature and pressure. For MSR, a steam-to-carbon ratio of α = 3 was used in calculations.

(STs). Evidently, temperatures well above 900 °C (higher for more endothermic MDR than for MSR) are required in order to obtain nearly complete CH_4 conversions (Fig. 3) which explains why SD and ST have been historically the systems of choice in solar reforming applications. Methane conversions also decrease with increasing pressure (due to the increase in total number of moles) and, though this decline is much less pronounced than the dependence on temperature, it is another important consideration in the design of solar reforming systems to be operated at the elevated pressures required for industrial applications. We note that Fig. 3 shows equilibrium (limiting) conversions, which are typically never reached in commercial applications due to kinetic limitations and restrictions of mass, heat and radiation transfer.

The distribution of products is important in applications where the solar-upgraded natural gas is used as a feedstock for the production of chemicals. Fig. 4 shows the equilibrium CO/H_2 ratio for both sets of reactions calculated as ϕ_{CO}/ϕ_{H_2} using eqn (9) or (16) for the MSR + WGS and MDR + RWGS processes respectively. At high temperatures, the equilibrium is mainly established by highly endothermic reforming reactions and the composition is dictated by their stoichiometry, *i.e.* $CO/H_2 \rightarrow 0.33$ and $CO/H_2 \rightarrow 1$ for MSR and MDR respectively (Fig. 4). For both the Fischer–Tropsch and the methanol synthesis processes, the ideal ratio is *ca.* $CO/H_2 = 0.5$. At intermediate temperatures, the CO/H_2 ratios depart from the reforming stoichiometry (due to exothermic WGS and mildly endothermic RWGS reactions), but the more desirable 0.33–1 range is never attained (Fig. 4). In the low temperature regime (<600 °C), a very small amount of CO is produced in the MSR–WGS process, while CO/H_2 ratios >2 are generated in the MDR–RWGS system. Consequently, parabolic troughs are rather unsuitable to directly produce syngas for chemicals because of both low CH_4 conversions (Fig. 3) and too low or too high CO/H_2 ratios (Fig. 4).

However, electrical power generation *via* gas turbines does not require complete CH_4 conversion and can tolerate virtually any H_2/CO ratio. Therefore, low temperature CSP systems (FR and PT) can be potentially used to upgrade methane for power generation, as well as high temperature systems (SD and ST). In this respect, the most important consideration is whether the natural gas heating value can be

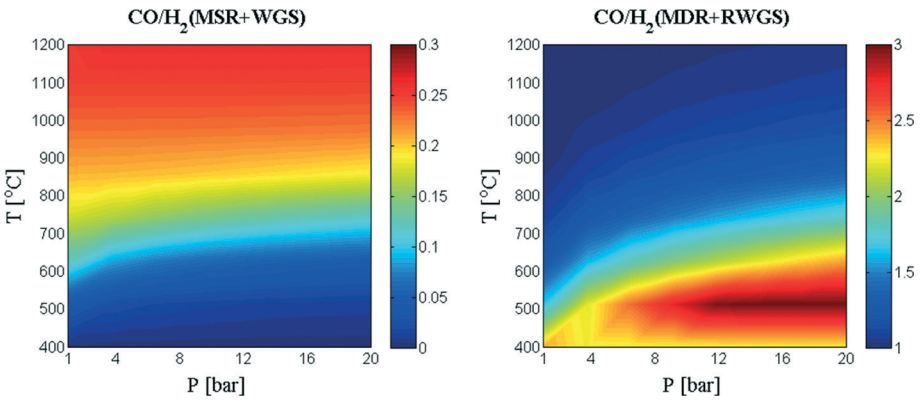

Fig. 4 Equilibrium CO/H_2 ratios for the combined MSR and WGS (left side) and MDR and RWGS (right side) processes are shown in the parametric domain of temperature and pressure.

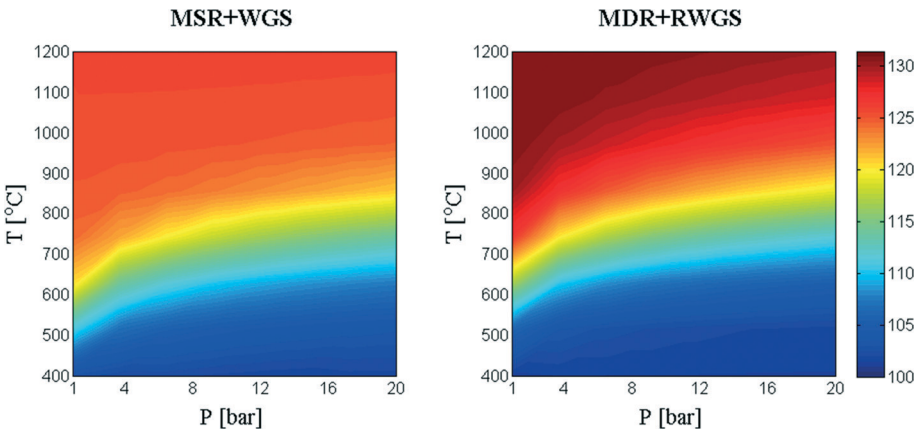

Fig. 5 Maximum fuel (CH_4) upgrade calculated based on low heating values (products of reforming *vs.* methane) and equilibrium compositions of the combined MSR and WGS (left side) and MDR and RWGS (right side) processes. The fuel upgrade values are shown in the parametric domain of temperature and pressure.

significantly upgraded by solar energy in a specific temperature range. The maximum values of fuel upgrade factor (UF, eqn (20) and (21), for MSR–WGS and MDR–RWGS respectively) by methane solar thermal reforming (MSTR) are shown in Fig. 5, as a function of the reforming temperature and pressure (100% refers to pure CH_4). These values were calculated using the previously calculated equilibrium conversions (from eqn (13) and (14) for MSR–WGS and eqn (18) and (19) for MDR–RWGS) and the low heating values (LHV) of CH_4, CO and H_2 (802.3, 241.8 and 283.2 kJ mol^{-1} respectively). As CH_4 is converted to CO and H_2, the heating value of the fuel increases as compared to pure CH_4. The maximum fuel upgrade for MDR is considerably higher than that for MSR (31.4% *vs.* 26.5% based on LHVs), due to the higher reaction enthalpy of MDR.

$$\mathrm{UF}_{\mathrm{MSR+WGS}}[\%] = 100\frac{(1-f_1)\mathrm{LHV}_{\mathrm{CH_4}} + f_2\cdot\mathrm{LHV}_{\mathrm{CO}} + (4f_1-f_2)\mathrm{LHV}_{\mathrm{H_2}}}{\mathrm{LHV}_{\mathrm{CH_4}}} \quad (20)$$

$$\mathrm{UF}_{\mathrm{MDR+RWGS}}[\%] = 100\frac{(1-f_1)\mathrm{LHV}_{\mathrm{CH_4}} + (2f_1+f_3)\mathrm{LHV}_{\mathrm{CO}} + (2f_1-f_3)\mathrm{LHV}_{\mathrm{H_2}}}{\mathrm{LHV}_{\mathrm{CH_4}}} \quad (21)$$

This analysis clearly shows that, under identical output conditions, the high temperature MSTR process can potentially save *ca.* 25–30% of the fuel (natural gas) as compared to the conventionally heated reforming that burns this fraction of the natural gas fed for process heating. The upgraded (solar) fuel can be then used for electricity generation using high efficiency conversion systems, such as gas turbines, or utilized as a chemical feedstock for chemical industry after gas conditioning. Although high temperatures are preferable from the thermodynamics point of view to maximize conversion, high-temperature CSP systems (ST and SD) require high capital cost investments. As such, low-temperature MSTR using PTs is a more attractive option since PTs are a relatively cheap and mature (commercialized on a large scale) technology.[5] Operating at low pressures at the upper limit of temperatures provided by PTs (550–600 °C) can upgrade *ca.* 10–15% of the fuel (Fig. 5), providing a significant increase in electricity output in applications using gas turbines, especially in a combined cycle (using both steam and gas turbines). It is important to note that, in addition to solar energy stored in chemical energy, there is also sensible heat originated from the solar energy (not accounted for in Fig. 5), which can be in principle recuperated and used for steam generation and natural gas preheating.

3. Methane reforming catalysis

Typical methane reforming catalysts consist of transition metal nanoparticles (*e.g.*, Ni) dispersed on a high surface area ceramic support (*e.g.*, Al_2O_3, preferably >100 m^2 g^{-1}). Simple synthesis routes such as wet impregnation, incipient wetness impregnation and co-precipitation are most commonly used for catalyst preparation. Important catalyst performance parameters, which are also relevant for methane solar thermal reforming (MSTR) are low cost, high activity and high durability, in addition to optimal catalytic pellet design, to provide low pressure drop, efficient heat and mass transfer, thermal stability and mechanical strength. With regards to MSTR, catalyst activity is a crucial factor for low-temperature applications (<600 °C), while at higher temperatures catalyst stability against sintering and thermal stresses becomes a dominant issue. Though numerous transitions metals, including nickel (Ni), are highly active in methane reforming at $T > 800$ °C, their stability against sintering is rather poor, while recurrent cooling and heating due to the cyclic nature of solar irradiation can lead to severe thermal stresses.

Industrial methane reforming catalysts are composed of polydisperse Ni nanoparticles supported on α-Al_2O_3 with metal loadings ranging from 10 and 18 wt% (an example is shown in Fig. 6), frequently promoted with alkaline earth metals, such as Mg. Ni has been historically the metal of choice for MSR because of its low price and reasonably high activity at intermediate and high temperatures above 700 °C. However, Ni-based catalysts are a poor choice for MSTR applications. Specifically, Ni is not suitable for MSR operating at low steam-to-carbon ratios or for MDR because it suffers from severe coking at these conditions (an example is shown in Fig. 7 (ref. 25)), which can be improved only to certain extent by modifying support.[26,27] In addition, for low temperature reforming (400–600 °C), Ni has insufficient intrinsic activity and suffers from fast deactivation *via* oxidative routes.[26]

Catalyst deactivation in CH_4 reforming reactions can occur by several pathways, namely sulfur poisoning, oxidation, sintering and coking. The first three routes have lower impact since sulfur can be removed from the reformer feed,

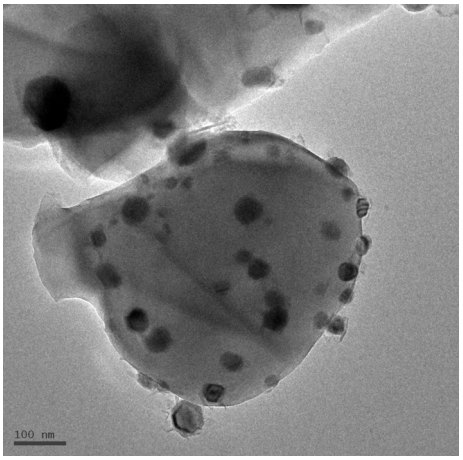

Fig. 6 TEM micrograph of a Ni/α-Al_2O_3 commercial catalyst (15 wt% NiO, Research Catalysts, Inc., www.catlyst-central.com) after 160 h on stream (MSR, T = 500–600 °C, P = 1–5 bar): Ni nanoparticles ranging from 35 ± 12 nm are dispersed on the α-Al_2O_3 support.

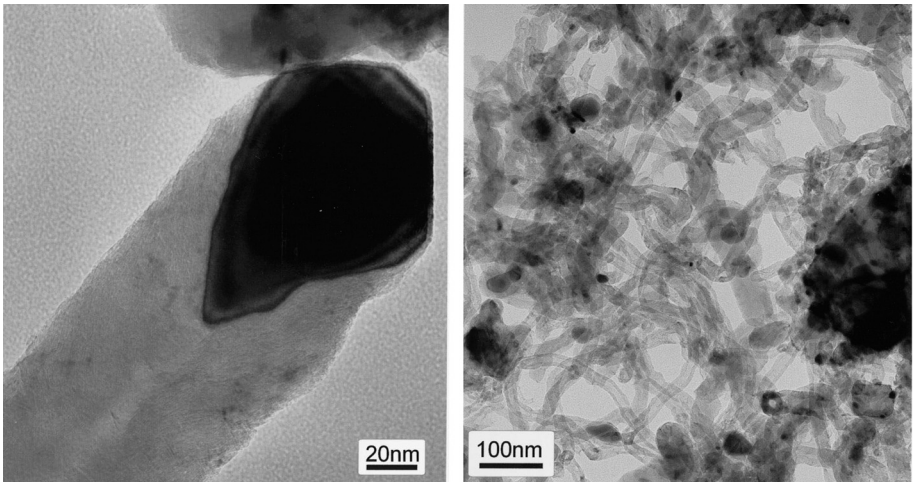

Fig. 7 TEM micrographs showing extensive formation of filamentous carbon (whisker carbon) during methane dry reforming over a Ni/MgO catalyst. Reprinted with permission from ref. 25. Copyright (2014) Elsevier.

oxidation does not occur to a significant extent under typical reforming condition (due to catalyst reduction in the H_2-rich reaction mixture), and sintering is typically slow. Carbon formation, on the other hand, remains a major challenge, particularly for Ni-catalyzed methane reforming.[19,21,22,28] Carbon deposition on the Ni surface first leads to the blockage of the active sites and subsequently to the formation of filamentous carbon (see Fig. 7 (ref. 25)), leading eventually to mechanical disintegration and catalyst bed clogging.

The development of new, active and stable, catalysts is therefore of critical importance for MSTR. Many other transition metals, including iron (Fe), cobalt (Co) and the platinum group metals (PGMs) can catalyze methane reforming.[26,29] However, Fe and Co deactivate rapidly by oxidation under the methane reforming conditions, while PGMs, which are typically highly active and stable, are much more expensive. Nevertheless, PGMs such as Ru, Rh, Ir, Pt and Pd have been extensively investigated for reforming applications, mostly for MDR.[29–31] Other directions include bimetallic catalysts (typically Ni promoted with a noble metal),[26,32] alternative catalytic materials such as transition metal carbides,[33,34] and modifying ceramic supports to reduce coking and sintering and to increase catalytic activity.[26,35,36] Next, we outline recent developments in methane reforming catalysis and critically discuss related challenges within the context of MSTR applications.

3.1. Density functional theory predictions

During catalytic methane reforming, CH_4 and either H_2O or CO_2 first adsorb and dissociate on the catalytic surface, react and then desorb as products (Fig. 8, MSR–WGS system is shown). While dissociation of CH_4 bonds requires metallic surfaces, H_2O dissociation can also occur on the ceramic support (Fig. 8), especially if the support features redox-active centers. The combined MSR–WGS reaction can be described in terms of elementary steps as shown in eqn (22).[37,38]

$$\text{MSR:}\quad CH_4 + H_2O \rightleftarrows CO + 3H_2$$
$$\text{WGS:}\quad CO + H_2O \rightleftarrows CO_2 + H_2$$

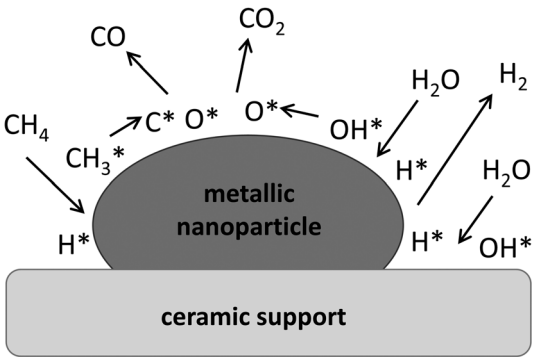

Fig. 8 Schematic (oversimplified) representation of the combined MSR–WGS process occurring on the surface of the supported metallic nanoparticle.

$$\begin{aligned}
&CH_4 + 2^* \rightleftharpoons CH_3^* + H^*\\
&CH_3^* + {}^* \rightleftharpoons CH_2^* + H^*\\
&CH_2^* + {}^* \rightleftharpoons CH^* + H^*\\
&CH^* + {}^* \rightleftharpoons C^* + H^*\\
&H_2O + 2^* \rightleftharpoons OH^* + H^*\\
&OH^* + {}^* \rightleftharpoons O^* + H^*\\
&2H^* \rightleftharpoons H_2 + 2^*\\
&C^* + O^* \rightleftharpoons CO^*\\
&CO^* \rightleftharpoons CO + {}^*\\
&CO^* + OH^* \rightleftharpoons HCOO^* + {}^*\\
&HCOO^* \rightleftharpoons CO_2 + H^*\\
&CO^* + O^* \rightleftharpoons CO_2 + 2^*
\end{aligned} \tag{22}$$

Note that there are several other possible pathways for CO formation *via* various adsorbed intermediates.[39] The MSR

reaction kinetics has been the subject of extensive research, which is beyond the scope of this review. We refer the reader to excellent publications on this topic.[36,37,40–44] Strong experimental and theoretical evidence exist supporting that CH_4 dissociation, *i.e.* C–H bond activation, is the single rate-determining step,[44] but other studies have suggested that CO formation can also be the rate-determining step depending on the reaction conditions.[37]

Density functional theory (DFT) can be applied to understand the underlying mechanisms of the methane reforming catalytic reaction and, importantly, to predict the reactivity of heterogeneous catalytic systems.[45,46] Specifically, potential energy diagrams can be readily constructed from the energy profiles of elementary steps for various catalysts (*e.g.*, Fig. 9a). This allows comparing relative stabilization of intermediates or transitions states for a particular set of reaction conditions.[37] DFT-based predictive modeling can be used to identify materials, including pure metals and their alloys, with high catalytic activity in MSR and MDR under conditions relevant to MSTR applications. The selected candidates can be then tested experimentally to verify that they indeed have high activity and, importantly, for stability against sintering, oxidation and coking deactivation, sulfur poisoning *etc.*

DFT studies of CH_4 reforming reactions on Ni surfaces have shown that the steps on a catalytic surface are more active sites for CH_4 dissociation,[37,39,47–49] For Ni, it was experimentally demonstrated that the reactivity of the stepped surface can be higher than that of the terraces by two orders of magnitude,[48] implying also that steps can serve as nucleation sites for carbon deposition.[49] DFT studies on Rh and Pt surfaces also have shown that stepped surfaces are much more reactive than planar surfaces of the corresponding metal.[50] Recent advances in electronic structure theory allow the screening of a large numbers of metal phases to find those with highest predicted rate, selectivity and stability.[37,39]

In addition to the *thermodynamic analysis* that provides the framework to create the potential energy diagram of the reaction steps (Fig. 9a), it is possible now to incorporate *reaction kinetics* and thus to calculate turn over frequencies (Fig. 9b).[37,39] DFT studies combined with experiments have shown that Ru and Rh are the most active among noble metals, while transition metals such as Ni, Co, Fe and Cu are much less active, Fig. 9b.[37] For noble metals, CO formation was identified as the rate-determining step, while for less noble metals the rate-determining step was dissociative adsorption of CH_4.

In a recent DFT study, a scan of catalytic activity for MSR was performed over a wide range of transition metals transition metal alloys.[39] Fig. 10 shows DFT predictions of turn over frequencies (TOFs) of CO production in MSR under industrial conditions for several inexpensive earth abundant metal alloys alongside with noble metals. For some alloys of Ni, Fe and Co, TOFs are predicted to be comparable to those of Ru and Rh. So far, the choice of catalyst for MSTR applications was predominantly restricted to Rh and Ru, due to their high activity and thermal stability. DFT predictive modeling is opening new avenues in the search for active and stable catalysts that can avoid the high cost associated with platinum group metals.

A DFT-based screening study of transition metal carbides (TMC) surfaces for MSR has been recently reported.[51] TMCs are known to exhibit "platinum-like behavior" for certain reactions.[52] The low cost associated with TMCs makes them attractive candidates to be used as alternatives to noble metals in MSR. Indeed, TMCs such as Mo_2C, WC and Co_6W_6C were found to be active and stable catalysts for MDR and MSR at elevated temperatures and pressures.[53,54] However, in the DFT study of TMC-catalyzed MSR,[51] most TMC surfaces that were investigated (*i.e.*, metal-terminated and oxygen covered TiC, VC, MoC and Mo_2C) were found to be unsuitable for MSR, since they were either prone to self-poisoning by the

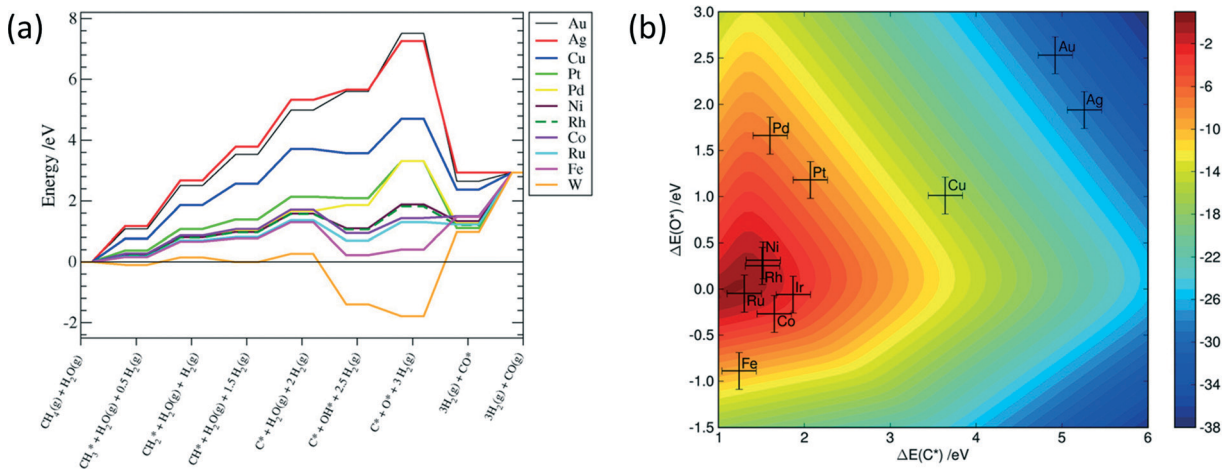

Fig. 9 DFT computation of MSR over stepped surfaces of various transition metals, showing (a) the potential energy diagram and (b) the two-dimensional volcano plot of the turn over frequency (log_{10}) as a function of O and C adsorption energy at 773 K and 1 bar. Reprinted with permission from ref. 37. Copyright (2014) Elsevier.

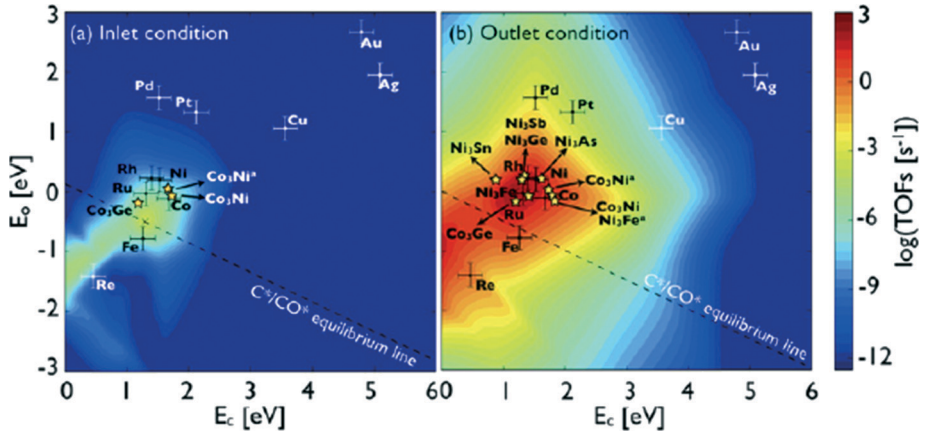

Fig. 10 DFT predictions of the turn over frequency (TOF) of CO production as a function of C and O binding energies (considering interaction between adsorbates), for MSR under industrial conditions. Inlet and outlet conditions correspond to T = 638 K and 1066 K and P = 14.3 bar and 12.2 bar. Reprinted with permission from ref. 39. Copyright (2014) IOP Publishing Ltd.

MSR intermediates or showed very high activation energies for some of the MSR elementary steps. Generally speaking, the main disadvantage of TMCs with respect to methane reforming is that the TMC surface is easily oxidized by either H_2O or CO_2. This limiting factor restricts the use of TMCs only to high temperature regimes wherein the intermediates can be more easily desorbed from the TMC surface and the surface can be more easily reduced. Such conditions are achieved using point focus solar collectors (ST and SD), providing a potential for the use of TMCs in high temperature MSTR.

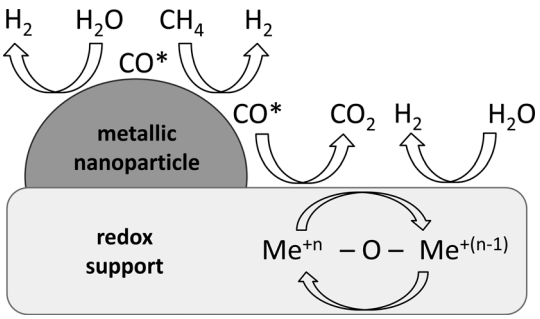

Fig. 11 A simplified schematic of the mechanism of MSR enhancement by redox support, by removal of the surface CO.

3.2. Catalyst supports

Catalyst performance can be significantly modified by the catalyst support either indirectly, by changing the metal dispersion and sintering behavior, or directly, by participating in adsorption and reaction steps. The role of support for low-temperature MSR has been recently reviewed, indicating the positive effects of some support materials (*e.g.* ZrO_2 and CeO_2).[26] In another recent review, progress towards the development of coke resistant Ni-based catalyst for MSR and MDR was outlined.[55] In addition to catalytic activity, the resistance of the catalyst to mechanical stresses and to high temperatures is of particular importance for MSTR, due to the intermittent nature of the solar energy source (day–night cycles and changing weather conditions) and the high process endothermicity.

An important feature for the support is oxygen storage capacity, which can be enhanced by the use of supports with redox properties (*e.g.*, CeO_2, ZrO_2). These supports can provide an additional source of oxygen for the reaction with adsorbed carbon to form CO, eqn (22), reducing therefore carbon deposition (a simplified mechanism is shown in Fig. 11).[26,56] Remarkably, there are experimental evidences that show a linear dependence of catalyst activity on the amount of metal sites located on the metal–support perimeter (Fig. 12),[35] suggesting that either the most active metal sites are those in contact with the ceramic redox support or that the surface oxygen flux from the support is the rate-determining step.

For the commonly used α-Al_2O_3 support, the rate of carbon deposition can be reduced by the use of alkali or

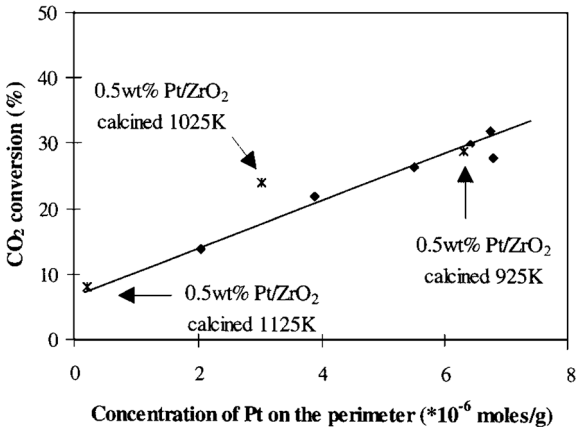

Fig. 12 Influence of the amount of accessible Pt on the activity of Pt/ZrO_2 catalysts for CO_2/CH_4 reforming at 875 K. Different Pt loadings (♦) and 0.5 wt% Pt calcined at different temperatures (*) are shown. Reprinted with permission from ref. 35. Copyright (2014) Elsevier.

alkaline earth metal promoters (*e.g.*, MgO), due to the enhanced uptake of oxidizing species. Other promoters (*e.g.*, Ce, La, Zr)[55,57] have been found to have a dramatic effect on the formation of coke over Ni-based catalysts, affecting the amount of carbon deposited and its morphology (graphitic, filamentous or amorphous).[58,59] In a recent work on low-temperature MSR on Ni-based catalysts, it was shown that, although coking is severe for Ni/SiO_2 and $Ni/\alpha\text{-}Al_2O_3$, promotion of Al_2O_3 with Mg can significantly reduce the rate of carbon deposition, and the use of Zn results in a dramatic improvement in the catalyst resistance to coking, Fig. 13.[59]

A variety of alternative supports have been investigated for MSR and MDR applications, including SiO_2, ZrO_2, TiO_2, La_2O_3, CeO_2, as well as mixed oxides.[26,55] Numerous studies have shown that ZrO_2 and CeO_2 are probably the best supports for Ni-catalyzed MSR[27,60,61] and for PGM-catalyzed MSR and MDR.[35,36,40–43,56,60,62–66] PGMs supported on La_2O_3 also exhibit high catalytic activity and stability in MDR.[67,68] On the other hand, SiO_2 was found to be a less suitable support for methane reforming applications.[35,69] Taken together, these studies show that the use of oxides such as CeO_2 and ZrO_2 provides important advantages in terms of resistance to sintering, catalytic activity and stability with respect to coke formation. Therefore, CeO_2 and ZrO_2 are good candidates for MSTR applications.

Zeolites have been also considered as support materials for Ni-catalyzed MSR[70] and MDR,[71] MDR catalyzed by bimetallic Ni–Rh catalyst,[72] and for Ru-catalyzed MDR.[73,74] Some properties of zeolites such as their microporous structure and exceptionally high specific surface area make them an interesting alternative. In addition, the high affinity of zeolites for CO_2 adsorption may be advantageous for MDR. Zeolite-supported PGMs or bimetallic catalysts (*e.g.* Ni–Rh) exhibit good catalytic performance in terms of conversion and stability,[72–74] but it is not clear whether their apparent stability is due to the zeolite support or to the PGM. Nickel catalysts supported on zeolites deactivate rapidly under the MDR conditions,[72] but zeolite surface modification with organo-silane groups prior to Ni impregnation can result in an active and stable Ni-based catalyst for MDR.[71]

Although a significant amount of work has been done and some promising candidates have been identified, systematic data on the performance of various supports in MSR and MDR is difficult to reconcile. Since TOF values, or at least conversion rates per catalyst amount, are not always reported, comparison of results from different groups is problematic. Correctly assessing catalytic activity is critical, particularly for low temperature MSTR applications where equilibrium limitations exist (Fig. 3–5). Kinetic limits are rarely considered, thus restricting tests to a specific (usually relatively low) space velocity. For MSTR applications, high space velocities are needed to maximize the throughput of a solar reactor in order to compensate for the higher capital cost investment. Long-term catalyst stability (in the order of hundreds of hours) is also very important but frequently omitted in academic studies.

3.3. Platinum group metals

PGMs, including Ru, Rh, Ir, Pt and Pd, have been identified as excellent reforming catalysts for MDR[29,31,36,40–44,63,67–69,75,76] and MSR.[56,60,64–66,77–81] The use of PGMs for CH_4 conversion is relevant in the context of partial oxidation and dry reforming, for which the use of Ni is excluded (because of oxidation and severe coking).[30] PGMs are much more stable against coking than Ni, exhibit much better dispersion and activity, and sinter much more slowly even at high temperatures. High catalytic activity is particularly important for low temperature MSTR applications (<600 °C). Progress towards the use of PGMs for low-temperature MSR was recently outlined.[26] For high temperature MSTR, high thermal stability of PGMs is an important advantage. However, the implementation of PGMs is hindered by the high costs associated with current catalyst formulations featuring relatively high PGM loadings, typically ranging from *ca.* 1–5 wt%.[41,42,60,62,63,78,81]

Numerous studies on the mechanism of PGM-catalyzed MDR and MSR have shown that, as in the case of Ni, the most important steps are dissociative adsorption of CH_4, H_2O and CO_2 and surface carbon oxidation (Fig. 8).[35,36,40–44,62,78,82] The identity of the rate-determining step is still strongly

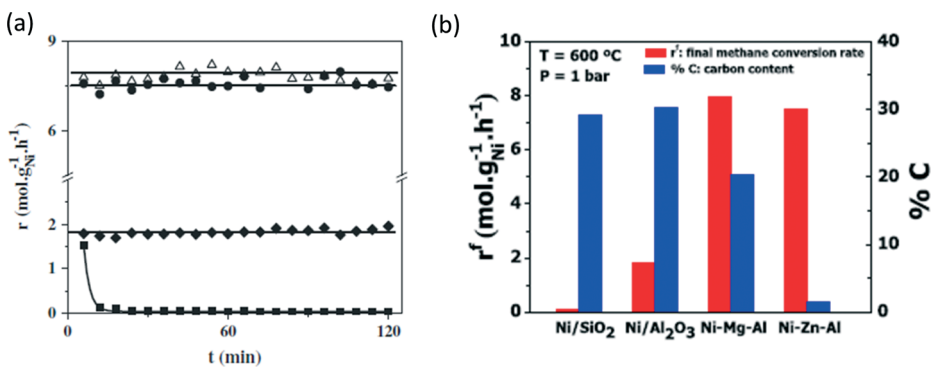

Fig. 13 Effect of support (squares, rhombi, triangles and circles correspond to Ni/SiO_2, Ni/Al_2O_3, Ni–Mg–Al and Ni–Zn–Al) on MSR methane conversion rate (a) and amount of carbon deposition (b). Reaction conditions: T = 600 °C, P = 1 bar, H_2O/CH_4 = 2. Reprinted with permission from ref. 59. Copyright (2014) Elsevier.

debated.[35–37,40–44,56,62,82] In a number of studies it was found that C–H bond activation is rate-controlling,[36,40–43] while other DFT-based studies suggested that the importance of various kinetic steps can vary depending on reaction temperature.[37,82] The fact that reforming rates typically increase with increasing PGM dispersion supports the importance of CH_4 dissociative adsorption, which is facilitated on low-coordinated edge and corner atoms characteristic for smaller nanoparticles.[36,41,50,78]

There is some controversy with regards to the order of activity of PGMs in reforming reactions. The following sequences were suggested: Ru ≈ Rh > Ni ≈ Pd ≈ Pt > Co in MSR,[83] Ru ≈ Rh > Ir > Ni > Pt ≈ Pd in MDR and MSR,[31,84] and Pt > Ir > Rh > Ru ≈ Ni in MDR and MSR.[36,40–44] While some authors agree on that Ru and Rh have the highest activity (Fig. 14a, b),[37,78] which is also supported by DFT studies (Fig. 9b),[37] other authors claim that Pt and Ir have much higher activities than Rh and Ru, in both MDR and MSR Fig. 15.[36] Experimentally measured turnover frequencies (TOFs) of PGM-based catalysts are shown in Fig. 14 and 15, as a function of metal phase dispersion.

TOFs of *ca.* 10–20 s^{-1} are typically reported for PGMs at 500–600 °C, while for Ni catalysts TOFs are an order of magnitude lower under same conditions (Fig. 14a). Optimizing catalyst support can improve dispersion and surface carbon oxidation (see section 3.2 for detailed discussion), but mechanistic studies show that TOFs are independent on the type of support,[36,41] indicating that reactions occurring on the support surface is not kinetically relevant and the role of support is rather indirect.

In the context of MSTR, Ru is an ideal PGM candidate due to its relatively low price among other PGMs (only *ca.* 100 times more expensive than Ni, while Rh, for example, is *ca.* 2000 times more expensive than Ni) and high activity (Fig. 9b and 14a). It is also stable against sintering at high temperatures (Ru melting point is 2334 °C) and against coking. The penalty of the much higher price of the PGM as compared to Ni can be compensated to some extent by the superior catalytic performance and lower PGM loadings (typical PGM loadings are *ca.* 1–5 wt% *vs. ca.* 10–18 wt% required for Ni). Nonetheless, PGM loading has to be drastically reduced by at least an order of magnitude (to *ca.* 0.1 wt% at least) for PGM-based catalysts to be of commercial interest. In this respect, studies describing ultra-low PGM loading catalyst performance under practical conditions are lacking, making it difficult to obtain a direct comparison with Ni-based catalysts over a wide range of operating conditions such as pressure, temperature and space velocity. Such information would be necessary in order to evaluate the potential of the use of PGMs in MSTR applications. In a recent work, catalytic activity of ultra-low loading Ru-based catalysts in low temperature MSR (400–600 °C) was systematically evaluated.[85] It was shown that the 0.15 wt% Ru/γ-Al_2O_3 catalyst has intrinsic activity which is two orders of magnitude higher than that of the commercial 12 wt% Ni/α-Al_2O_3 catalyst, featuring also excellent stability in a wide range of operating parameters.

3.4. Nickel-based bimetallic catalysts

A potentially cheaper alternative to the use of PGMs is coupling Ni with other metals in order to improve resistance to coking and sintering and to increase catalytic activity. Many Ni-based bimetallic catalysts have been investigated so far for reforming reactions, using noble metals (Pt, Pd, Rh, Au, Ag)[32,55,58,72,86–93] and other transition metals (Cu, Co, Fe, Mo, Sn)[26,32,94] as a secondary phase. Typical precious metal loadings used for bimetallic Ni-based catalysts range from *ca.* 0.5–1.5 wt% to as high as 4 wt%.[58,88–93] Due to the limited miscibility of Ni with other metals, the two metals typically do not interact strongly by forming an alloy, but rather the second metal acts as a dopant or as a separate phase.

When a PGM is used as a promoter, its surface sites can facilitate dissociative adsorption of CH_4 and initiate rapid dissociation of H_2 and H_2 spillover (migration of surface atomic hydrogen) onto the catalyst support and adjacent NiO surfaces. This process can facilitate the reduction of the

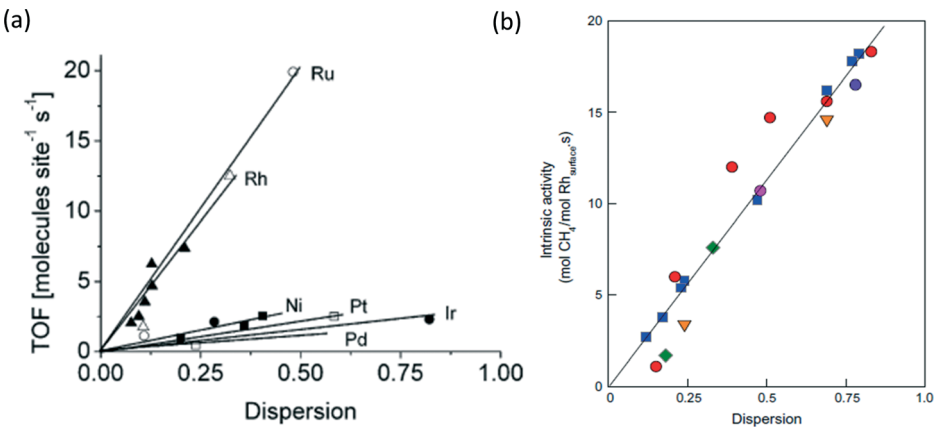

Fig. 14 MSR TOF over (a) Ru, Rh, Pt, Pd, Ir and Ni supported by ZrO_2 and Al_2O_3 at 1 bar, 500 °C, H_2O/CH_4 = 4 and (b) Rh supported by ZrO_2 (squares), CeO_2 (circles), $CeZrO_2$ (triangles) and SiO_2 (rhombi) at 1 bar, 500 °C, H_2O/CH_4 = 3. TOF is shown as a function of the catalyst metal phase dispersion. Reprinted with permission from ref. 37 and 78. Copyright (2014) Elsevier.

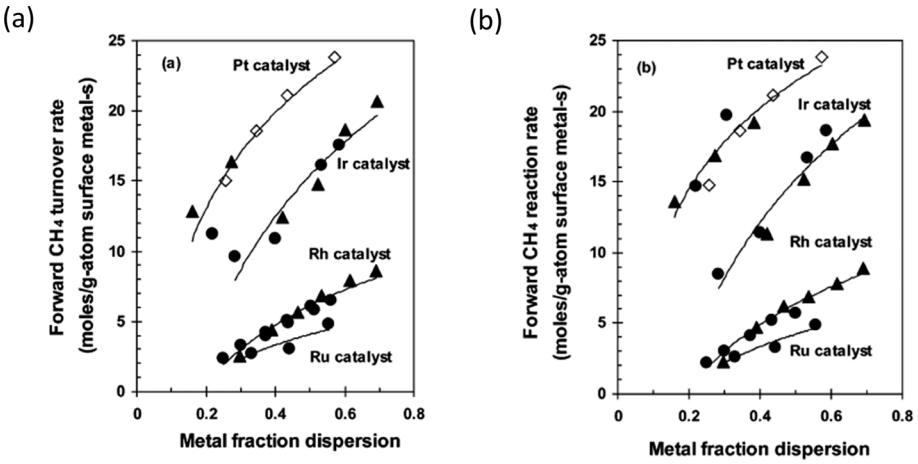

Fig. 15 Methane conversion turnover frequencies (TOF) in (a) MDR and (b) MSR at 600 °C, over Pt, Ir, Rh and Ru supported by ZrO_2 (triangles), ZrO_2–CeO_2 (rhombi) and γ-Al_2O_3 (circles). TOF is shown as a function of the metal phase dispersion. Reprinted with permission from ref. 36. Copyright (2014) American Chemical Society.

NiO surface.[26,55] Moreover, the addition of PGMs to Ni typically increases the overall metal dispersion, creating, therefore, more active catalytic sites.[26,55] Addition of small amounts of Ag and Au can lead to blockage of highly active catalytic sites on the Ni surface (step and edge sites) that are mainly responsible for the nucleation of carbon formation, hindering therefore coke formation. However, this approach can also lead to a substantial decrease in catalytic activity.[26,32,58,86]

Addition of non-precious metals (*e.g.* Sn, Fe, Co, Cu) to Ni can also reduce the susceptibility to the carbon formation nucleation by changing the electronic properties of the metallic surface, *i.e.* by displacing Ni atoms from the highly active step and edge sites.[32] Bimetallic Ni–Co and Ni–Cu formulations were shown to be much more stable against coking than pure Ni.[95–97] For example, very little carbon formation was found in a 2000 h stability test at high space velocity over magnesium aluminum oxide supported Ni–Co catalyst, Fig. 16a.[96] Recently, it was demonstrated that Zr–Al_2O_3 supported bimetallic Ni–Cu alloys are also resistant to carbon formation at high space velocities Fig. 16b.[95]

Doping of Ni with noble metals can provide important benefits in terms of catalytic activity and stability for MSTR applications that typically involve high temperatures. The high price and limited availability of precious metals used as a second phase can be compensated to some extent by the mentioned above benefits. However, due to relatively high loadings, which are currently used (typically *ca.* 0.5–1.5 wt%), the implementation of this approach still needs to be validated from the economic point of view. Moreover, while the addition of noble metals to Ni typically provides a significant improvement in the catalyst stability, it may result in substantial loss of catalytic activity.[39] Further research is required to identify the most suitable secondary metal. Systematic evaluation of the potential of Ni-based bimetallic alloys for MSTR applications will also require information regarding the relative order of intrinsic catalytic activity of various metals in a bimetallic configuration. To date, however, such

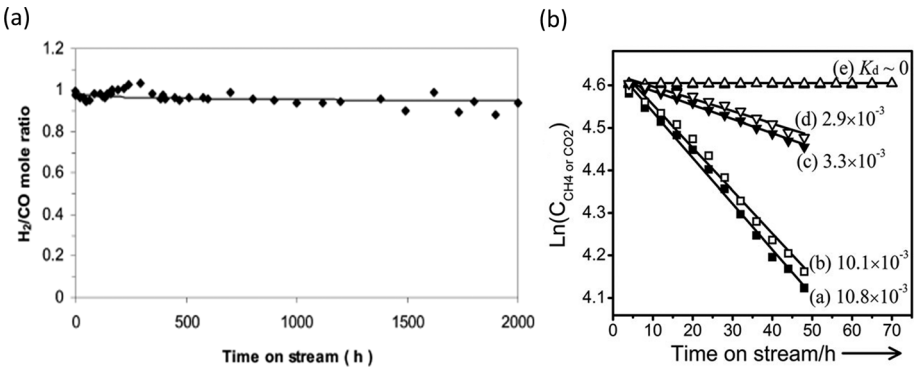

Fig. 16 MDR over (a) Ni–Co catalyst supported on magnesium aluminum oxide (H_2/CO ratio *vs.* time on stream is shown) at 750 °C, 1 bar and with GHSV = 110 000 mL (g^{-1} h^{-1}) and (b) over Ni/Al_2O_3 (a, b), Ni–Cu/Al_2O_3 (d, c) and Cu–Ni/Zr–Al_2O_3 (e) catalysts at 800 °C, 1 bar and with GHSV = 120 000 mL (g^{-1} h^{-1}), showing CH_4 and CO_2 conversion rate *vs.* time on stream. Reprinted with permission from ref. 95; Copyright (2014) Wiley and ref. 96; Copyright (2014) Elsevier.

assessments are difficult since TOF values are not always reported, the lowest concentration of the heterometal dopant are not investigated, and bimetallic catalysts are not evaluated in and compared to typical industrial conditions.

3.5. Transition metal carbides

Transition metal carbides (TMCs) are a class of earth-abundant catalysts that feature Pt-like surface electronic properties.[52] TMCs are typically synthesized by carburization of corresponding transition metal oxides (TMOs) at high temperatures, using either CO, CH_4 or higher hydrocarbons as a source of carbon. Synthesis routes for preparation of high surface area unsupported TMCs powders have been in development since the 1980s.[98–100] Recently, it has been shown that WC, Mo_2C and bimetallic Co_6W_6C are active and stable catalysts for MDR.[33,34,53,54,101–104] Unsupported WC, Mo_2C and Co_6W_6C were found to be active and, importantly, stable catalysts for MDR at high temperatures and elevated pressures,[33,34,53,54,101,102] Fig. 17. The reported order of catalytic activity for single metal TMCs was $Mo_2C \approx WC > VC > NbC > TaC$,[101] while turnover rate of Mo_2C was only an order of magnitude lower than that obtained with Ru/Al_2O_3.[33] Importantly, the rate of carbon deposition for Mo_2C and WC was very low and comparable to that of PGMs (Rh, Ir, Ru and Re), which was attributed to the similarity of the electronic structure between Mo_2C and Ru and between WC and Pt.[33] The role of support in the catalytic performance of supported Mo_2C catalysts in MDR was also investigated and it was found that the relative order of catalyst stability was $Mo_2C/Al_2O_3 > Mo_2C/ZrO_2 > Mo_2C/SiO_2 > Mo_2C/TiO_2$.[104]

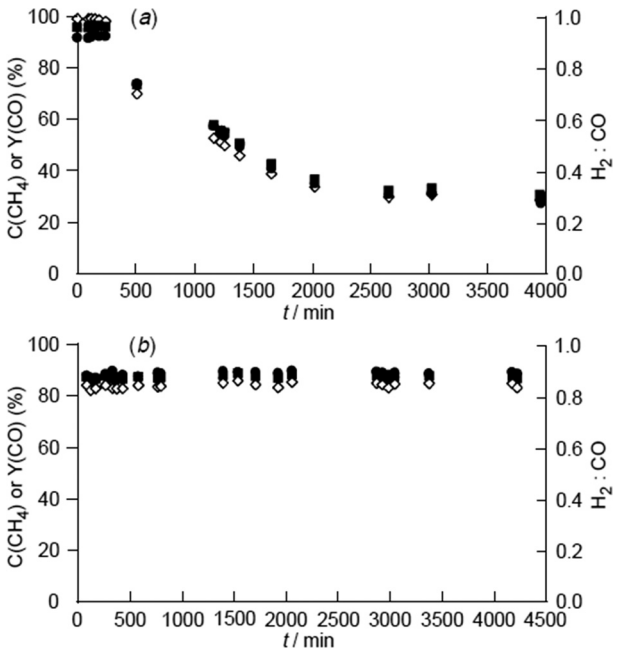

Fig. 17 Catalyst stability during MDR over unsupported Mo_2C at T = 1220 K, CH_4/CO_2 = 1, GHSV = 2800 h^{-1} and pressure of (a) 1 atm and (b) 8.3 atm. CH_4 conversion (rhombi), CO selectivity (squares) and H_2/CO (circles) ratio are shown. Reproduced from ref. 53.

Fast TMC catalyst deactivation was observed at atmospheric pressure (Fig. 17a), and was attributed to the oxidation of the TMC surface by dissociative adsorption of CO_2 on the catalyst surface followed by oxidation of the TMC by oxygen atoms. An example of the deactivation mechanism for molybdenum is shown in eqn (23).[101] While oxidation of the TMC occurs at relatively low temperatures (500–850 °C), the transformation of the transition metal oxide (TMO) back into the TMC occurs only at high temperatures (>850 °C). Thus, oxidation and reduction (recarbidation) at the surface are in competition and catalyst deactivation is dictated by relative stability of the TMO or instability of the TMC under the given set of MDR conditions. The increased catalyst stability at elevated pressures can thus be attributed to the longer contact time (for a given GHSV), allowing the slower carbidation reaction to reach equilibrium.[101]

$$\begin{aligned} Mo_2C + 5CO_2 &\rightleftarrows 2MoO_2 + 6CO \\ 2MoO_2 + 5CH_4 &\rightleftarrows Mo_2C + 4CO + 10H_2 \end{aligned} \quad (23)$$

The two main advantages of TMC-based catalysts with respect to MSTR and MDR in particular are high stability against sintering and resistance to coking. However, further work is required in order to understand the nature of the active phase formed under MDR conditions, since it is not clear if the surface is metal or carbide terminated at temperatures above 850 °C. This understanding can help improve the activities of TMCs, which are currently significantly lower than those obtained with PGMs. Since the surface of TMC-based catalysts undergo oxidation at low temperatures under CH_4 reforming conditions,[51] they are rather unsuitable for low temperature MSTR applications. The use of TMCs could be restricted to high temperature MDR, *i.e.* to the conditions when the oxidation is less severe and intermediates can more easily desorb from the TMC surface. Such conditions are definitely relevant for high temperature MSTR using point focus solar collectors (solar dishes and solar towers).

3.6. Catalyst selection

While the selection of proper catalyst for a particular MSTR application will depend on several factors, the operating temperature regime will have the highest impact. Table 1 below qualitatively summarizes the most critical performance properties for three classes of catalysts over the three temperature regimes obtainable by solar concentrators. From the point of view of catalytic activity and stability, the obvious choice of the active phase is platinum group metals (PGMs) that provide excellent performance over all temperature ranges, with a minor tendency to oxidative deactivation at low temperatures. However, PGMs are very expensive and scarce which makes their implementation for MSTR very problematic, unless the metal loading is drastically reduced, at least to *ca.* 0.1 wt%, while still providing high activity and stability.[85] Ni-based catalysts provide reasonable performance in the high temperature regime, but have a strong tendency towards carbon formation, limiting their use to high steam-to-carbon

Table 1 Activity and stability of different types of catalysts[a]

Catalytic property in methane reforming	Nickel-based			Platinum group metals			Transition metal carbides		
	LT	MT	HT	LT	MT	HT	LT	MT	HT
Catalytic activity	Low	Fair	High	High	High	High	Low	Fair	High
Coking resistance	Low	Low	Low	High	High	High	High	Fair	Fair
Sintering resistance	Fair	Low	Low	High	High	Fair	High	High	Fair
Oxidation resistance	Low	Fair	High	Fair	High	High	Low	Fair	High

[a] Legend: LT – low temperature range (400–600 °C) obtainable by parabolic troughs, MT – medium temperature range (600–900 °C) covered by solar dishes and solar towers, HT – high temperature range (>900 °C) exclusively provided by central receivers (solar towers).

ratios. Such MSTR applications can be still relevant, if the problem of handling large amounts of excess steam is resolved. An interesting alternative is transition metal carbides, which can provide fair performance in the intermediate temperature regime and good performance for high temperature MSTR applications.

4. System design for methane solar thermal reforming

The earth receives about 173 PW (1.74×10^{17} watts) of solar radiation at the top of the atmosphere. Approximately 30% is reflected back to space and a significant fraction is absorbed by clouds and oceans so that only about 40% reaches the planet's surface (this amount is still much higher than the rate of energy consumption of the entire planet). The irradiance available for terrestrial use is on order of magnitude of 1 kW m^{-2}.[2,5] Such fluxes can only generate low temperatures which are insufficient for applications involving solar thermochemical conversion. It is therefore essential to use optical concentration devices (see Fig. 1 and section 1 for details),[2,5] which implies special requirements for catalyst and reactor design. In this section, we review the state-of-the-art of the reactor design and catalyst performance for MSTR.

4.1. Reactor engineering aspects of solar thermal reforming of methane

Solar thermal energy can be integrated into a reforming system either indirectly or directly. The indirect approach is similar to conventional CSP plants in the sense that a heat transfer fluid is used to conduct solar heat from the receiver to the point of use. The difference is that in MSTR systems the heat transfer fluid is used to heat the reformer. Since MDR or MSR require temperatures higher than 800 °C to achieve high methane conversions (Fig. 3), conventional heat transfer fluids such as steam and synthetic oil cannot be used, requiring compressed hot gas (*e.g.*, air) instead. Molten salts, most of which are only stable below 550 °C, can be mainly used for low temperature MSTR applications (see section 4.2).

In directly irradiated reforming systems, solar radiation is focused onto the catalytic element, which implies that the reformer is an integrated unit that combines the solar receiver and the catalytic bed in one system. PT and FR technologies are limited to $T < 600$ °C, therefore, regardless of the reactor type, higher temperatures required for MDR and MSR effectively limit the choice of solar concentrator to ST and SD. Since the reformer is directly irradiated with sunlight, heating is much more efficient due to the radiative character of heat transfer in contrast to conventional conduction–convection, enabling operation at temperatures as high as *ca.* 1000 °C. Various solutions of solar energy integration into reforming systems have been outlined in a recent review.[105]

MSTR systems based on indirect approach do not necessary require any special reactor design. The only essential difference from the conventional reforming is the source of heat, which is now originated from sun. Therefore, tubular geometry, similar to that of industrial reformers, can be used in indirect MSTR systems.[106–113] Direct MSTR, on the other hand, implies many special requirements to the design of the reformer which should effectively integrate a solar receiver with a catalytic element. Such reformer has to fulfill requirements regarding the solar receiver/absorber (low reflectivity, low emissivity and high thermal shock resistance), as well as requirements regarding the catalytic bed (high activity and stability against sintering and coking). Because of the intermittent nature of the solar radiation, the catalyst should feature high thermal stability and to be capable of operating under highly dynamic thermal conditions. The catalytic unit should be designed in such a way that concentrated solar radiation can be efficiently absorbed without significant losses. While high temperatures are thermodynamically favored for high methane conversions, high-temperature operation is disadvantageous from the point of view of materials selection and catalytic element. Several types of directly-irradiated solar thermal reformers have been developed and demonstrated in solar tests.[114–133]

4.1.1. Indirect MSTR: sodium heat pipe reformer. The use of sodium (Na) heat pipe has been suggested to transfer the solar heat from the receiver to the reformer, Fig. 18.[110–113] In this concept, concentrated sunlight is used to evaporate liquid Na contained in an evacuated chamber. The sodium vapor condenses on the reformer tubes in the chamber releasing the heat of vaporization to drive the endothermic reforming reaction, and the liquid sodium is collected back into the absorber by gravity. The approach is in principle indirect, since there is no direct irradiation of the catalytic

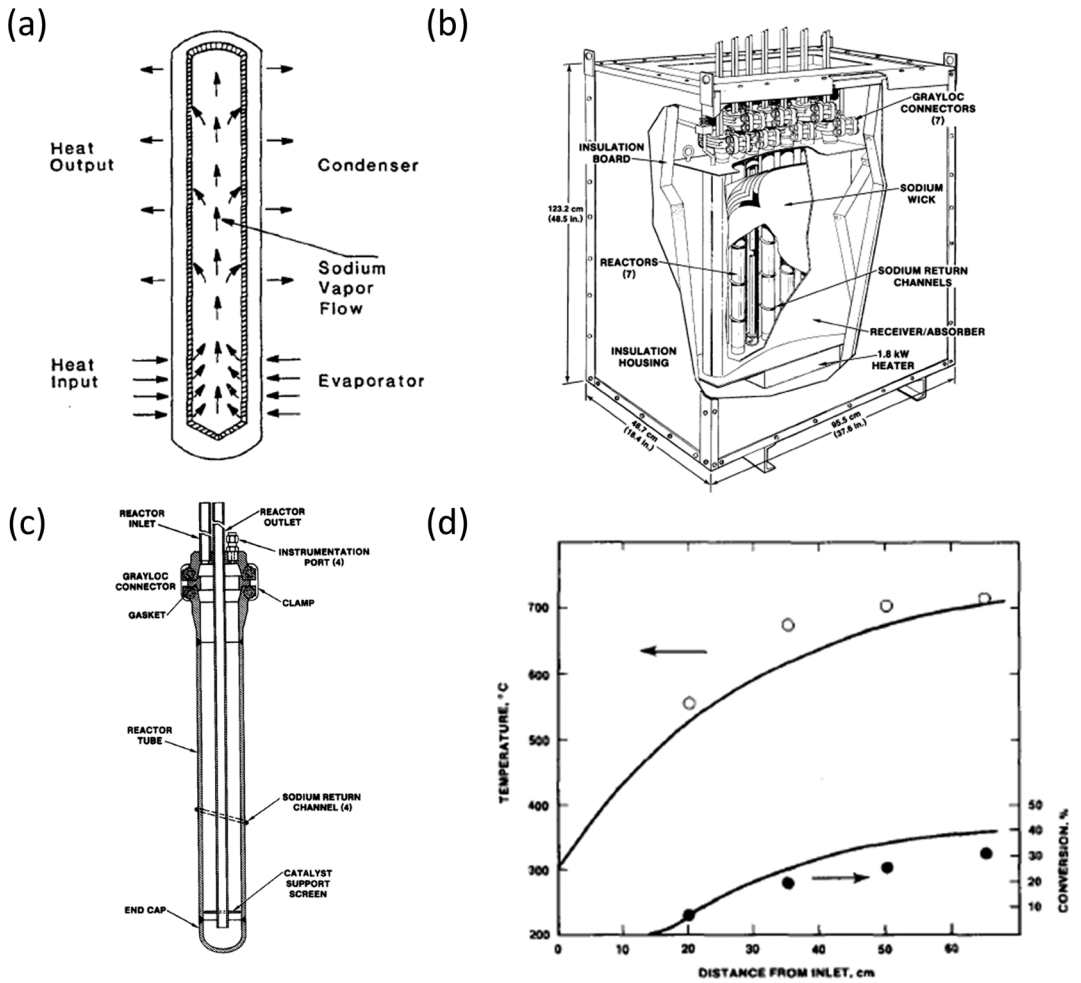

Fig. 18 Sodium reflux heat pipe receiver reactor for MSTR: (a) sodium heat pipe concept; (b) schematic drawing of the sodium heat pipe receiver/reactor containing several reformer tubes; (c) details of a single reformer tube; (d) results of solar-driven MDR experiment using 0.5 wt% Rh/γ-Al_2O_3 catalyst, showing temperature and conversion profiles along the reformer tube (lines show model prediction). Reprinted with permission from ref. 111 and 113. Copyright (2014) Elsevier.

bed, but the solar receiver and the catalytic reformer are integrated in a single unit. A main advantage of this system is the excellent heat transfer characteristics of evaporating and condensing sodium, which results in a more uniform temperature distribution throughout the chamber. It has been reported that the flammability of sodium vapors is a safety concern.

The concept was tested first for MSR using the Na heat pipe reactor with a single reformer tube (20 kW capacity), using a commercial 14 wt% Ni/Al_2O_3 catalyst and simulated solar radiation (infrared lamps).[111,112] The reformer was successfully operated at 600–900 °C for many cyclic runs simulating daily insolation profiles. Near-equilibrium methane conversion was achieved and no catalyst deactivation was observed when operating with feed steam-to-carbon ratios higher than 2.5. Further work focused on MDR and, since Ni-based catalyst deactivate rapidly in MDR because of coking, Ru/γ-Al_2O_3 and Rh/γ-Al_2O_3 (commercial, 0.5 wt% PGM) catalysts were tested.[110] The Rh/γ-Al_2O_3 catalyst was found to be more active and stable and was selected for final demonstration using a real CSP facility using ST, Fig. 18b–d.[113] The solar reformer was operated at 720–825 °C, 2–5.5 atm, CO_2/CH_4 = 1.1–1.2 and methane flow rates ranging from 530–2500 SLPH (standard liter per hour). Methane conversions of 50–70% were achieved with an energy input of 1.5–7.8 kW. Experiments were prematurely terminated because of operational failure of the sodium evaporator. No detailed information on catalyst performance was provided.

4.1.2. Indirect MSTR: molten salt gas–liquid reformer. The use of solar molten salts (mixtures of alkali metal nitrates and carbonates) as an intermediate heat transfer fluid has been proposed for MDR applications, Fig. 19.[134,135] The high heat capacity of molten salts allows for their use as (sensible) heat storage and can in principle compensate for fluctuations in solar irradiation due to meteorological factors. However, molten salts which are used in conventional CSP plants (*e.g.* $NaNO_3/KNO_3$) have low melting point and decompose above 600 °C, effectively limiting their applications to temperatures <550 °C. Other molten salts have much higher melting point and can be used in high temperature

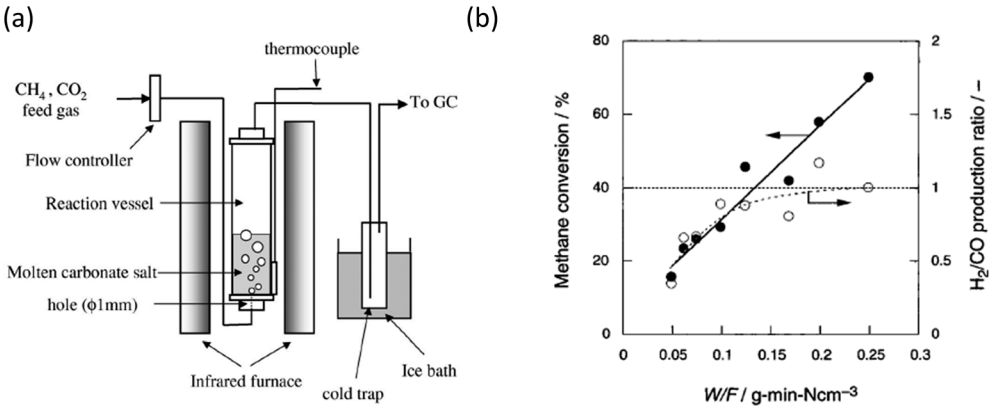

Fig. 19 Cylindrical liquid bed reactor (a) for MDR using molten salt as a heat transfer fluid and Ni/Al_2O_3 catalyst dispersed in the molten salt and the reformer performance after 4 h of operation (b) in terms of CH_4 conversion and produced H_2/CO ratio as a function of *W*/*F*. *W* and *F* represent the weight of the Ni/Al_2O_3-molten salt mixture and flow rate of CH_4/CO_2 feed, respectively. *W* and *F* ranged from 30 to 50 g and 200–800 N cm^3 min^{-1}. The catalyst/molten salt weight ratio was 1. Reprinted with permission from ref. 134; Copyright (2014) American Chemical Society and 135; Copyright (2014) Elsevier.

MSTR applications, for example, the K_2CO_3/Na_2CO_3 1 : 1 w/w system melts at ~710 °C.[134,135]

The reformer based on K_2CO_3/Na_2CO_3 molten salt has been implemented for MDR using non-precious metal catalysts, Fig. 19. The catalyst powder and the salt were mixed and placed in a lab-scale stainless steel cylindrical reactor and heated to 950 °C using infrared furnace (Fig. 19a). The feed (CH_4 and CO_2) was bubbled through the molten salt containing the catalyst. Ni, Cu, Fe and W supported on α-Al_2O_3 (20 wt% metal loading) were tested, as well as unsupported FeO catalyst. Ni/α-Al_2O_3 was found to be the best among tested transition metal catalysts, while FeO also showed catalytic activity in MDR, decomposing CH_4 and CO_2 into CO, H_2 and H_2O by redox action. As expected, CH_4 conversion increased with increasing residence time, Fig. 19b. Although the experiments were conducted at very low space velocities (GHSV $<$ 1600 ml (g^{-1} h^{-1}), Fig. 19b) and temperature/pressure conditions wherein nearly full methane conversion was expected, incomplete CH_4 conversions were obtained. These results suggest the presence of significant mass transfer limitations that severely limit the applicability of this approach. In addition, excessive amounts of soot particulates were found in the reactor after the seven-day operation of recurrent heating and cooling, indicating severe coking.

4.1.3. Indirect MSTR: molten salt tubular reformer. A composite material containing the Na_2CO_3 molten salt loaded with ceramic particles (to increase heat capacity) was used as a heat transfer medium and MDR was performed in a double-walled tubular receiver/reformer (~1 kW capacity), with a 2 wt% Ru/γ-Al_2O_3 commercial catalyst (spherical pellets with a diameter of 3 mm) loaded in the inner tube and the Na_2CO_3/MgO composite molten salt filled in the shell, Fig. 20a.[133] Experiments were conducted at atmospheric pressure and *ca.* 920 °C using simulated solar radiation (electric furnace), Fig. 20b. Nearly complete CH_4 conversion was obtained using CO_2/CH_4 = 3 in the feed and residence time of 0.3 s (GHSV = 12 500 h^{-1}), Fig. 20c, d. Due to the high heat capacity of the heat transfer medium, it was possible to maintain CH_4 conversion at a significantly high level for 1 h without heating (simulating cloud passages), Fig. 20c. The tubular double-walled design using a composite molten salt/ceramic is promising, due to its simplicity and the high heat capacity of the heat transfer/storage medium. It is unclear, however, whether it is possible to effectively concentrate sun radiation on such a receiver and more complex design solutions would be probably required to integrate the tubular receiver/reformer into a real CSP system (ST and SD). The use of 2 wt% PGM loading is clearly not feasible from the economic point of view, but the reformer design is flexible in this respect, allowing incorporation of any catalyst.

4.1.4. Direct MSTR: volumetric receiver-reactors. Early designs of direct MSTR systems were based on a tubular geometry.[114] In the directly irradiated tubular receiver/reformer, the concentrated solar radiation is absorbed by an exterior metallic wall of the reactor, which transfers the solar heat to the catalytic bed inside the tube. More advanced solutions are based on volumetric receiver–reformers (also called direct catalytic absorption receiver reactors).[115–126,128–132] In a volumetric receiver–reformer, concentrated solar radiation illuminates directly (through a transparent window) the catalyst bed, a ceramic monolith (honeycomb, ceramic or metallic foam) coated with a catalyst. Ceramic and metallic foams that provide high gas permeability and, at the same time, effective and uniform absorption of solar radiation are preferable over honeycomb monoliths. Such solar reformers can in principle operate at very high temperatures (even as high as 1000–1100 °C), since the temperature limit of conventional metal tubular reformers is eliminated and due to much higher heating rates by direct solar irradiation. High temperatures are advantageous thermodynamically and kinetically (high equilibrium conversions and reaction rates) but imply restrictions related to the thermal stability of the ceramic monolith and the catalyst. Two most common

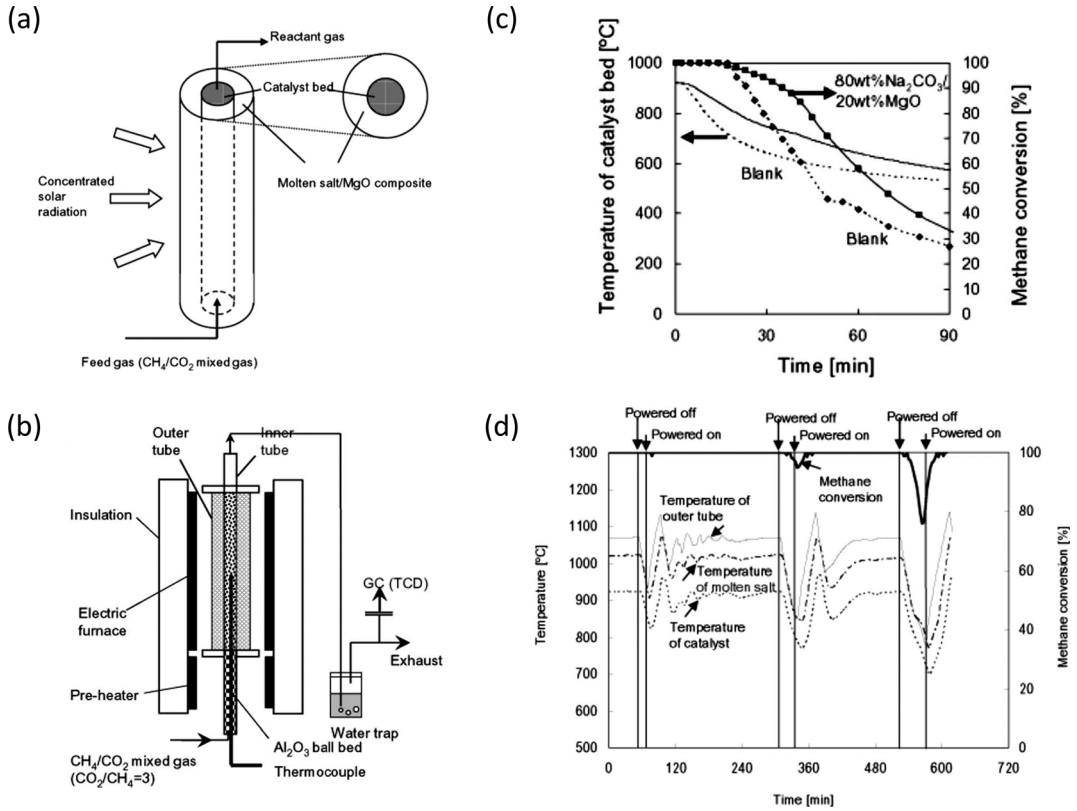

Fig. 20 Solar thermal MDR using a tubular double-walled receiver/reformer and 2 wt% Ru/γ-Al_2O_3 catalyst (indirect MSTR): (a) design of a double-walled reactor tube; (b) experimental setup; (c, d) transient variations of reactor temperature and conversion during the cooling mode (c) and on/off cycles (d). Reprinted with permission from ref. 133. Copyright (2014) American Society of Mechanical Engineers.

catalysts used in direct MSTR studies are rhodium (Rh) and ruthenium (Ru). Both are highly active (see section 3.3 for detailed discussion) and have excellent thermal stability, which is of crucial importance for direct MSTR applications.

Solar MDR was successfully demonstrated using a direct absorption receiver reactor and a 150 kW capacity parabolic solar dish.[119,121] The reformer integrated into a CSP system (Fig. 21a, b) contained the directly irradiated catalytic element, a porous alumina (92 wt% α-Al_2O_3 and 8 wt% mullite) foam disk coated with Rh catalyst (Fig. 21c). The foam disk was first coated with γ-Al_2O_3 to increase the specific surface area (by an order of magnitude) and then with Rh (0.2 wt%). The absorber temperatures ranged from 550–1100 °C, depending on insolation conditions such as passing clouds. Interestingly, it was observed that during the cloud passage the insolation dropped from ~600 W m^{-2} to almost zero, showing that solar reforming is very challenging.

Though the reformer demonstrated good performance, absorbing *ca.* 100 kW of solar power and giving methane conversions up to 70%, major issues with the catalytic element degradation and catalyst deactivation were encountered. Considerable surface dislocation and cracks of random length and direction were observed after the reformer operation due to high thermal stresses. In addition, the Rh content was very non-uniform and significant sintering of the Rh nanocrystallites was observed. In the untested catalytic element Rh was homogeneously dispersed on the surface as 2–6 nm nanoparticles, while in the tested absorber the Rh nanoparticles size ranged from 8–28 nm on the front surface to 4–14 nm on the back of the absorber. This indicated development of strong temperature gradients across the catalytic element during the operation. As a result of the significant loss of the active surface, Rh catalyst deactivated, in addition to the mechanical fracture of the foam disk. Notably, no carbon formation was observed.

To improve the resistance of the catalytic absorber against thermal stresses, it was suggested to use metallic foams, as an alternative to fragile ceramic foams.[126] Rh, Ru and Ni were applied as the active catalytic phase on the alumina coated or non-coated Ni–Cr–Al foam disk, which was used as the catalytic absorber. In the MDR experiments with solar-simulated heating (Fig. 22a), Rh and Ru catalysts showed better performance than Ni (Fig. 22b) using 2–5 wt% metal loadings. Methane conversion of 73% was achieved at GHSV = 8500 h^{-1} at atmospheric pressure, while ~50% of the incident irradiation reaching the absorber was stored as chemical enthalpy.

Another material that can be used as a catalytic absorber is silicon carbide (SiC). Solar thermal MDR was successfully demonstrated using ceramic foam catalytic absorber reformer (Fig. 23) integrated in a central receiver solar tower facility.[124] Two ceramic foam structures, made from α-Al_2O_3 and SiC ceramics, with γ-Al_2O_3 as a high surface area support material

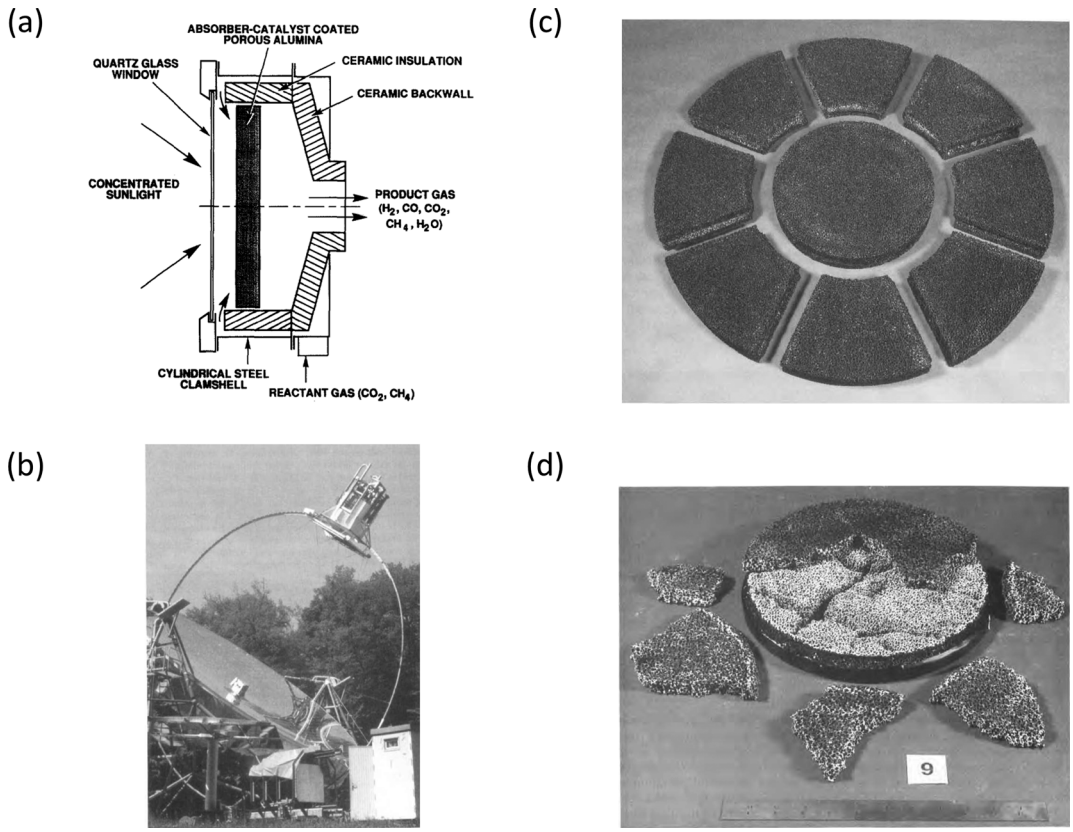

Fig. 21 Schematic of the direct catalytic absorption receiver reactor (a), parabolic dish solar concentrator with the installed volumetric receiver–reformer (b) and the catalytic absorber element (alumina foam coated with Rh/γ-Al_2O_3 catalyst) before test (c) and after MDR operation (d). Reprinted with permission from ref. 119 and 121. Copyright (2014) Elsevier.

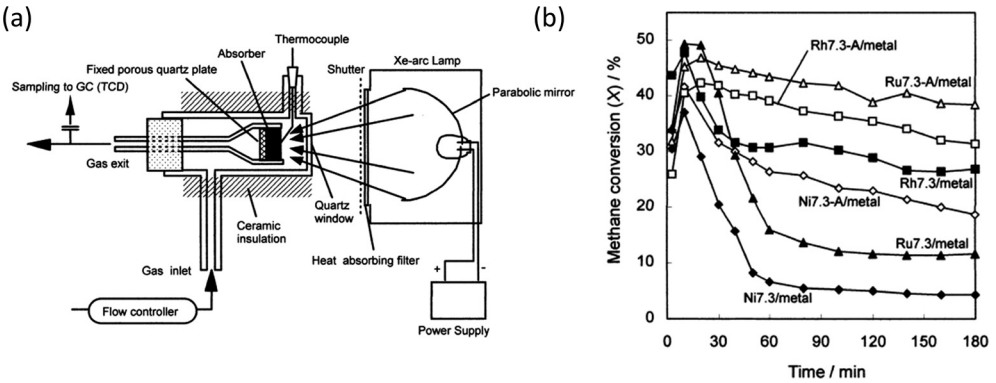

Fig. 22 Schematic of experimental setup for solar-simulated MDR using a Ni–Cr–Al metal foam absorber (a) and transient CH_4 conversion obtained with different catalysts deposited on the metallic foam directly (closed symbols) or as γ-Al_2O_3 supported (open symbols) (b). Operating conditions: CO_2/CH_4 = 1, T = 870 °C, P = 1 atm pressure and GHSV = 8500 h^{-1}. Reprinted with permission from ref. 126. Copyright (2014) American Chemical Society.

and Rh as an active metal phase, were tested. The solar receiver–reformer absorbed *ca.* 200–300 kW of solar power. Typical operating temperatures ranged from 700–800 °C and methane conversions over 80% were reached at 3.5 bar. The catalytic elements were characterized prior to solar experiments and afterwards. The reformer performed very well during solar operation, but significant coke deposition that resulted in catalyst deactivation was observed, Fig. 23b.

Though for some time research in the field of MSTR focused predominantly on MDR (mostly due to the difficulty of the excess steam utilization in MSR), some recent studies demonstrated the potential of MSR in MSTR applications. A lab-scale MSR was investigated under direct irradiation from a solar simulator using a volumetric receiver–reactor with quartz window and SiC foam catalytic absorber, Fig. 24.[132] The ceramic foam was coated with Al_2O_3 and, consequently,

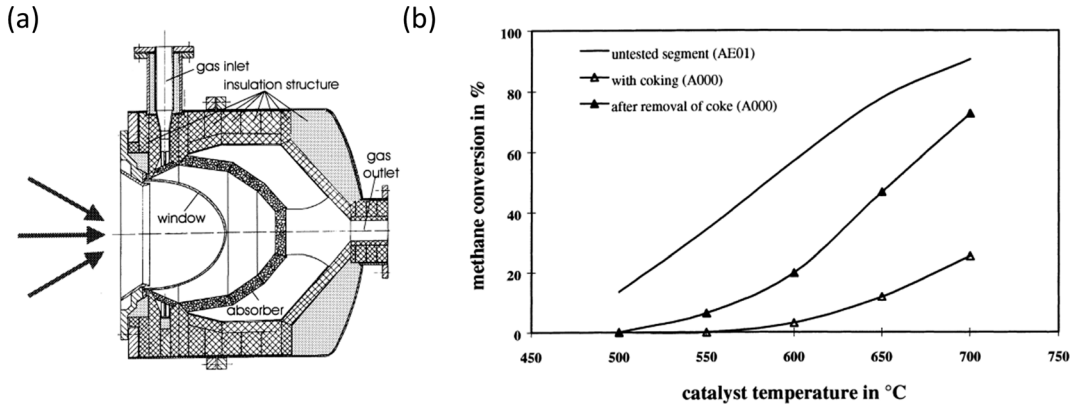

Fig. 23 Direct catalytic absorber receiver reactor for MDR: (a) schematic of 300 kW solar receiver–reformer with α-Al_2O_3 or SiC ceramic foam used as an absorber and catalyst support and (b) CH_4 conversion obtained during the characterization of the catalytic element before and after the solar test, showing intensive coking. Reprinted with permission from ref. 124. Copyright (2014) Elsevier.

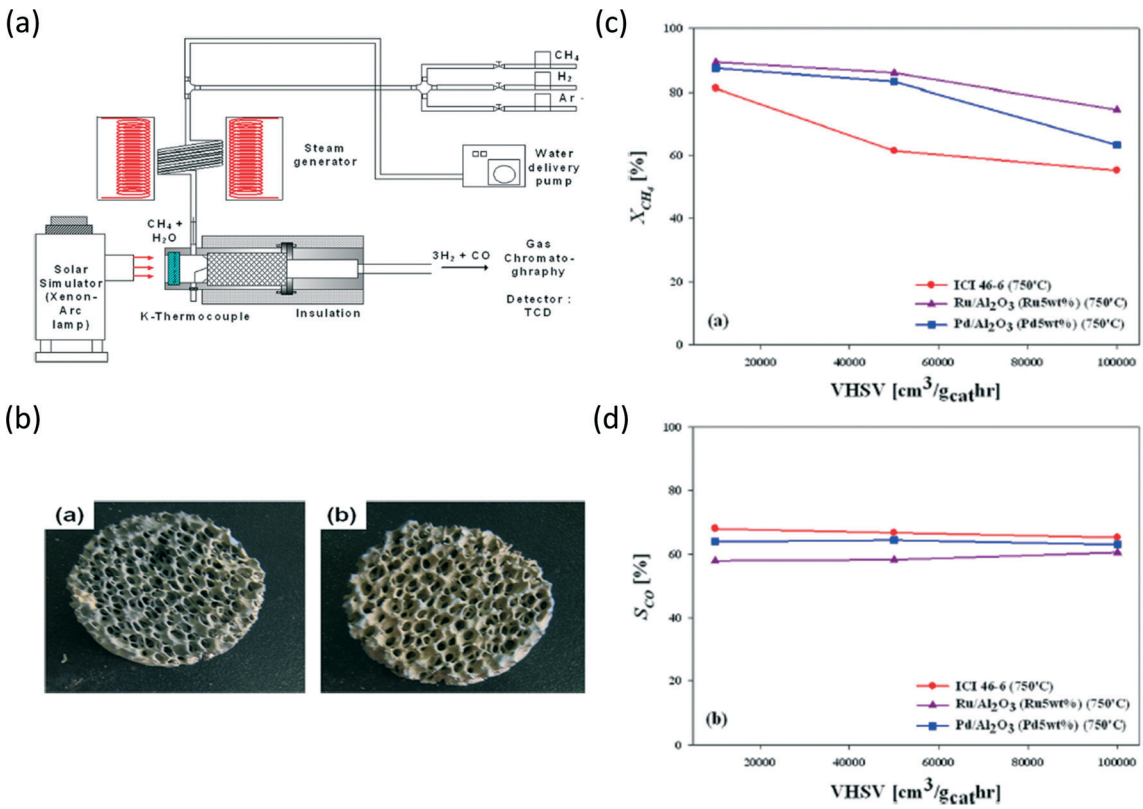

Fig. 24 MSR in a volumetric receiver–reactor using a SiC ceramic foam absorber and different supported catalysts (Pd, Ru and Ni): (a) schematic diagram of the experimental setup used for solar-simulated MSR; (b) photographs of the SiC foam coated with catalyst by spray and wash-coat methods and (c, d) effect of GHSV on the reformer performance at 750 °C, atmospheric pressure and H_2O/CH_4 = 3 (in the feed), in terms of CH_4 conversion (c) and CO selectivity (d). Reprinted with permission from ref. 132. Copyright (2014) American Society of Mechanical Engineers.

with three different catalysts: Ni (commercial), Ru and Pd (5 wt% PGM loading). The reformer was operated at 750 °C, atmospheric pressure and H_2O/CH_4 = 3 in the feed. All three catalysts showed very similar performance and no coke formation was observed. Importantly, the reformer was tested over a range of space velocities and only relatively minor decrease in methane conversion was observed even at high space velocity (Fig. 24c, d). It should be noted, however, that very high PGM loading was used (5 wt%).

Recently, an alternative design for the catalytic absorber was suggested, based on an array of ceramic pins used as catalyst support (Fig. 25).[129,131] Such configuration was shown to be very stable against thermal stresses and the volumetric receiver–reformer with the "Porcupine" type catalytic

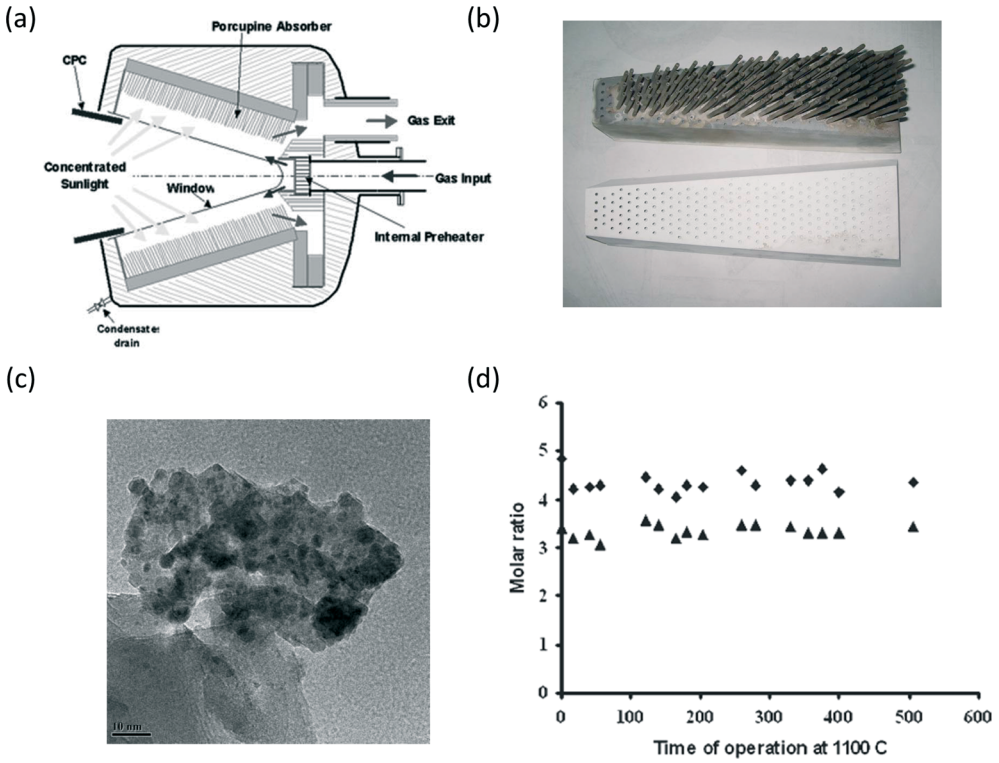

Fig. 25 MSR in a volumetric receiver–reformer with an array of ceramic pins used as an absorber element: (a) schematic view of the reformer; (b) two (alumina) catalytic absorber sections before and after inserting ceramic pins; (c) TEM image of the 2 wt% Ru/MnO–α-Al_2O_3 spent catalyst and (d) stability test showing solar reformer performance over a time period of 500 h at 1100 °C, in terms of H_2/CO (rhombi) and H_2/(CO + CO_2) ratios. Reproduced from ref. 129. Reprinted with permission from ref. 131. Copyright (2014) American Society of Mechanical Engineers.

absorber was successfully tested for MSR using central receiver solar tower facility.[131] Ru supported on MnO promoted α-Al_2O_3 (6 wt% PGM) was selected as a catalytic system, due to its high activity, stability against coking and relatively low price. Promotion with MnO effectively hindered sintering of Ru nanoparticles even at temperatures as high as 1100 °C. It should be noted that the Ru loading used were too high for commercial applications.

4.2. Low temperature solar thermal reforming of methane

Low temperature MSTR (<600 °C) has a number of important advantages over high temperature solar reforming systems. It was recently suggested to use PTs to provide the heat for MSR using indirect MSTR, with molten salts as heat transfer and storage medium.[106–109] The indirect MSTR approach allows for easy incorporation of solar reformers into the existing PT CSP plants and the reformer design does not have any special requirements, Fig. 26. In fact, tubular reformer geometry very similar to industrial reformers can be used. The use of PTs and molten salts intrinsically results in low methane conversions. Another issue is low activity of Ni-based catalysts at low temperatures and their tendency to fast oxidation deactivation. Carbon formation that at low temperatures occurs mainly by exothermic Boudouard coking and reverse gasification, eqn (5) and (6), is also a concern. The use of hydrogen selective membranes to shift the MSR equilibrium towards H_2 generation is a promising approach (Fig. 27). Selective separation of H_2 by Pd-based membranes can allow obtaining nearly complete conversions even at low temperatures.[24] The price of Pd and the membrane durability are the main obstacles.

4.3. Catalyst selection in solar thermal reforming systems

Historically, catalyst selection in MSTR applications was based mainly on its stability against coking and sintering, the two major problems encountered in Ni-catalyzed methane reforming. Table 2 below outlines progress in implementation of different methane reforming catalysts in various MSTR systems, summarizing section 4.1. A typical choice of the active phase is Rh or Ru, due to their exceptional stability against coking and sintering and high activity. However, the high cost associated with current active phase loadings makes the use of PGMs impractical for MSTR applications. Catalysts based on Ni can be still used in MSTR, but only for MSR applications with high steam-to-carbon ratio, which is disadvantageous from the point of view of solar facilities design and operation. Alternatives are clearly required, including (but not restricted to) PGM-based catalysts with ultra-low metal loadings (*e.g.*, below 0.1 wt%), bimetallic and

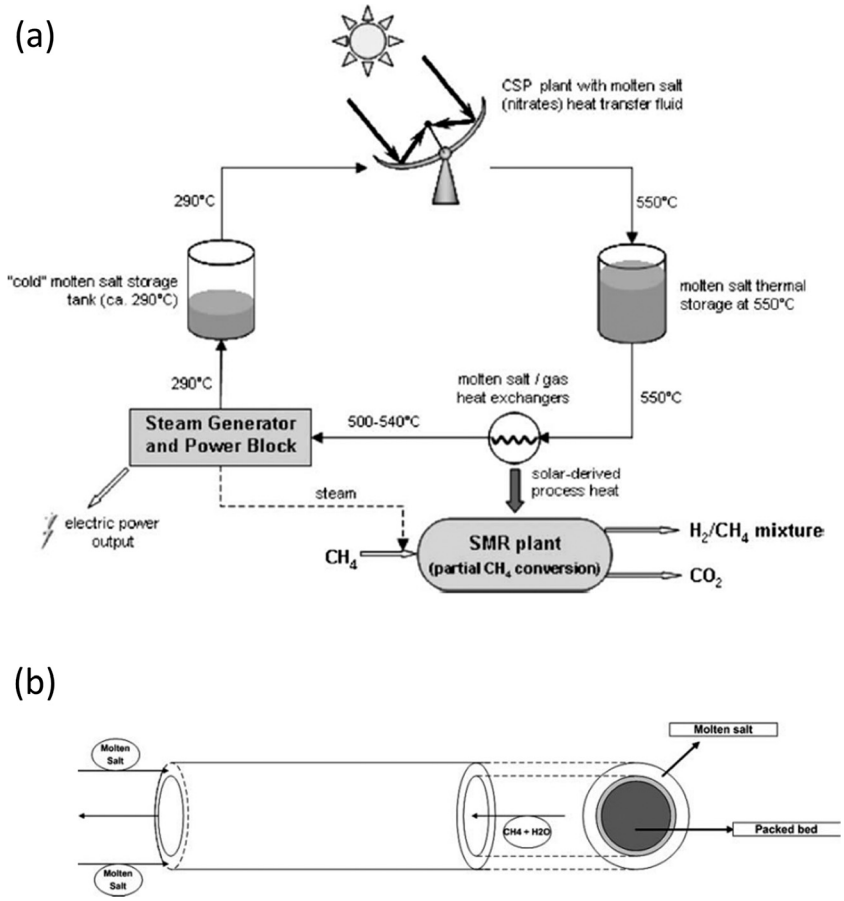

Fig. 26 The concept of low temperature MSR using indirect MSTR with molten salts as a heat transfer fluid: (a) simplified scheme of the hybrid PT CSP plant with molten salt loop, heat storage coupled to low temperature SMR and electrical power generation plant and (b) schematic of the molten salt-heated tubular catalytic packed bed reformer. Reprinted with permission from ref. 106; Copyright (2014) Wiley and ref. 107; Copyright (2014) International Association for Hydrogen Energy.

multimetallic catalysts based on cheap transition metals and catalysts based on transition metal carbides.

5. Concluding remarks and future perspectives

Solar thermal catalytic reforming of methane is a promising route to increase the efficiency of fossil fuels utilization. This is particularly true for the countries that have abundant solar radiation and large resources of natural gas. Solar reforming can be integrated into power generation cycles or used for production of important chemical feedstocks from methane. The most promising approach is methane steam reforming and, while methane dry reforming may be attractive due to the potential of carbon dioxide sequestration, carbon dioxide streams are not readily available. An interesting alternative is combined steam-dry reforming, which can be used when natural gas has significant fraction of carbon dioxide.

Though the potential of solar reforming is clear, its practical implementation is very challenging. There are many technological issues that were not resolved yet, even after several decades of quite intensive research. As a result, widespread commercialization of solar reforming has not been achieved, although important proof-of-concept facilities are already operational. Among drawbacks are high capital cost investments of solar installations, problems related to thermal stability of the reformer materials and, particularly, shortcomings related to solar thermal reforming catalysis.

The conventional methane steam reforming catalyst formulations are well established, but commercial Ni-based catalysts, though cheap and reasonably active at high temperatures, are unsuitable for solar thermochemical conversions. Ni-based catalysts have low activity and suffer from fast oxidation deactivation at low temperatures, moderate sintering at high temperatures, and, mainly, coking. Coke formation is suppressed in industrial settings by using high steam-to-carbon ratios, but using excess steam in solar thermal applications is problematic because of low throughput in infrastructure with high capital cost.

Solar thermal reforming of methane calls for the development of new catalysts. Ideally, these next-generation catalysts should be cheap, active and stable against oxidation, coking, sintering and poisoning. Unfortunately, the most active and stable catalysts are based on expensive noble metals. New directions involve using bimetallic and multimetallic configurations (alloys) that provide alternative surface electronic properties to modulate reactivity and offer different levels of

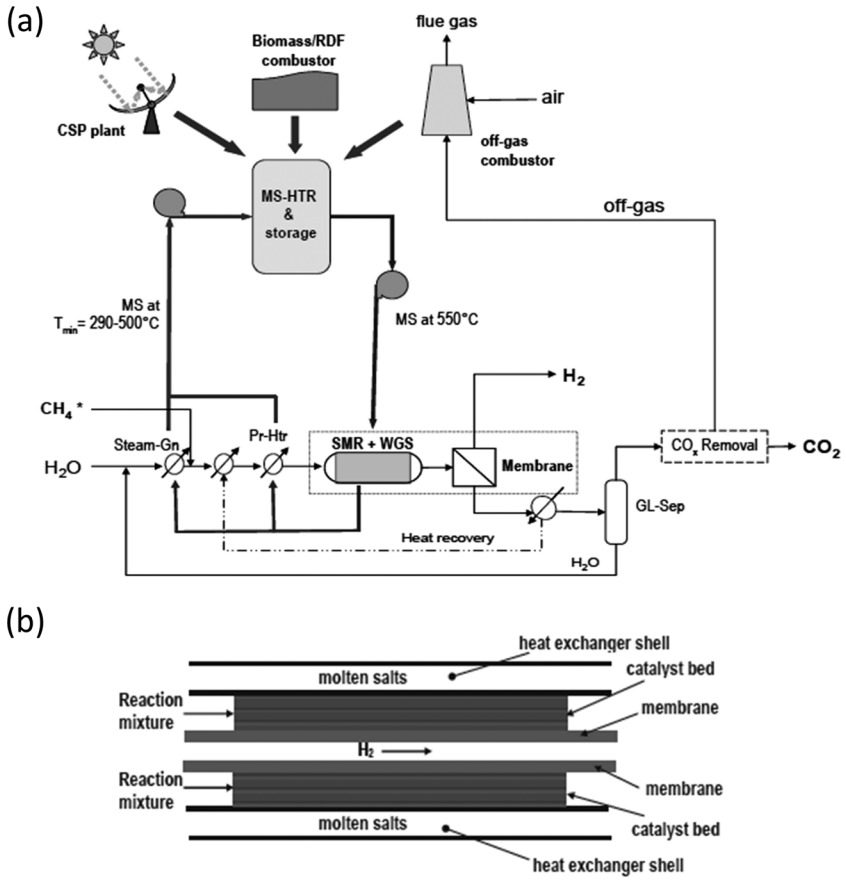

Fig. 27 Hydrogen generation by indirect MSTR *via* low temperature MSR, CSP, molten salts as heat transfer fluid (a) and catalytic membrane reactors (b). Reprinted with permission from ref. 109. Copyright (2014) AIDIC Servizi S.r.l.

Table 2 Performance of different types of catalysts in various solar thermal reforming systems[a]

Catalyst	Reactor	CSP	P_I, kW	Reaction	Feed rate	T, °C	Ox/C	f	Durability
14 wt% Ni/α-Al_2O_3 (ref. 111)	HPTR	*smd*	6	MSR	1350 SLPH	600–900	2–6	0.5–1	Stable
0.5 wt% Rh/α-Al_2O_3 (ref. 113)	HPTR	ST	2–8	MDR	1000–5700 SLPH	650–800	1.2	0.5–0.7	Reformer failure
20 wt% Ni/α-Al_2O_3 (ref. 134)	MSB	*smd*	—	MDR	1000–1500 mL (g_{cat}^{-1} h^{-1})	950	1	0.6–1	Coking (soot formation)
20 wt% Fe/α-Al_2O_3 (ref. 135)	MSB	*smd*	—	MDR	1000–1500 mL (g_{cat}^{-1} h^{-1})	950	1	0.3	Coking (soot formation)
2 wt% Ru/γ-Al_2O_3 (ref. 133)	MSTR	*smd*	1	MDR	5000–12 500 h^{-1}	920	3	0.9	Stable
0.2 wt% Rh/γ-Al_2O_3 (ref. 119 and 121)	DCAR	SD	100	MDR	20 000–35 000 SLPH	550–1100	1	0.4–0.7	Sintering, fracturing
5 wt% Rh(Ru)/γ-Al_2O_3 (ref. 126)	DCAR	*smd*	3–5	MDR	8500 h^{-1}	870	1	0.7	Stable
2–20 wt% Rh/γ-Al_2O_3 (ref. 124)	DCAR	ST	200–300	MDR	—	700–860	1.4	0.8	Coking
5 wt% Ru(Pd)/γ-Al_2O_3 (ref. 132)	DCAR	*smd*	1	MSR	10 000–100 000 mL (g_{cat}^{-1} h^{-1})	500–750	3	0.2–0.9	Stable
2–6 wt% Ru/α-Al_2O_3 (ref. 129 and 131)	DCAR	ST	10–20	MDR	6000–14 100 SLPH	720–900	1.2	0.4–0.8	Stable

[a] Legend: HPTR – (sodium) heat pump tubular reactor, MSB – molten salt bath, MSTR – molten salt tubular reformer, DCAR – direct catalytic absorption reformer, CSP – concentrated solar power, ssf – solar simulator furnace, P_I – irradiation power, SLPH – standard liter per hour, Ox/C – oxidant (H_2O or CO_2)-to-methane carbon ratio, f – methane conversion.

stability. Some of them, hopefully, are not that expensive, sufficiently active and stable enough for solar thermal reforming applications. Another direction is optimizing the catalyst support to improve metallic phase dispersion and to enhance carbon containing species oxidation and, again, various metal–ceramic support configurations can provide many degrees of freedom. The use of transition metal carbides is an attractive alternative to catalysts based on platinum group metals. Novel nanostructured catalyst designs could allow drastic reduction of the active phase loading, which can make noble metals relevant and economically competitive for solar thermal reforming applications.

An attractive route for methane upgrading is low temperature solar thermal reforming using parabolic trough solar concentrators. The parabolic trough technology is mature and relatively inexpensive but limited to temperatures below 600 °C. Though thermodynamic equilibrium dictates relatively low methane conversions for these temperatures, this limitation can be overcome by the use of hydrogen selective separation membranes. Moreover, high methane conversions are not necessary required for power generation applications, wherein natural gas upgraded by solar energy is used as a fuel for gas turbines. Low temperature regime allows for the use of cheap materials and simple designs for the reformer but imposes special requirements for the reforming catalyst which has to be very active, stable to oxidation and resistant to coking at the same time. Development of such catalysts would rely on density functional theory predictions (to identify most active metals and metal alloys) and careful design of the catalyst morphology at nanoscale, to optimize metal–support interactions and to reduce the active phase loading.

Abbreviations

BC	Boudouard reaction
CSP	concentrated solar power
DFT	density functional theory
FR	Fresnel reflector
LHV	low heating value
MC	methane cracking
MDR	methane dry reforming
MSR	methane steam reforming
MSTR	methane solar thermal reforming
PGM	platinum group metal
PSA	pressure swing adsorption
PT	parabolic trough
RG	reverse gasification
RWGS	reverse water gas shift
SD	solar dish
ST	solar tower
TOF	turn over frequency
TMC	transition metal carbide
TMO	transition metal oxide
WGS	water gas shift

Acknowledgements

The authors highly appreciate and acknowledge the support of King Fahd University of Petroleum and Minerals through the research grant # R12-CE-10 offered by KFUPM-MIT Clean Water and Clean Energy Research Collaboration Center.

References

1 R. Messenger, D. Y. Goswami, H. M. Upadhyaya, T. M. Razykov, A. N. Tiwari, R. Winston and R. McConnell, in *Handbook of energy efficiency and renewable energy*, ed. F. Kreith and D. Y. Goswami, CRC Press, Boca Raton, FL United States, 2007, pp. 1–63.
2 M. Romero-Alvarez and E. Zarza, in *Handbook of energy efficiency and renewable energy*, ed. F. Kreith and D. Y. Goswami, CRC Press, Boca Raton, FL United States, 2007, pp. 1–98.
3 T. A. Reddy, R. Battisti, H. Schweiger, W. Weiss, J. H. Morehouse, S. Vijayaraghavan and D. Y. Goswami, in *Handbook of energy efficiency and renewable energy*, ed. F. Kreith and D. Y. Goswami, CRC Press, Boca Raton, FL United States, 2007, pp. 1–134.
4 M. Z. Jacobson, *Energy Environ. Sci.*, 2009, **2**, 148–173.
5 M. Romero and A. Steinfeld, *Energy Environ. Sci.*, 2012, **5**, 9234–9245.
6 A. Steinfeld, *Sol. Energy*, 2005, **78**, 603–615.
7 W. R. Wagar, C. Zamfirescu and I. Dincer, *Int. J. Hydrogen Energy*, 2011, **36**, 7002–7011.
8 P. V. Zedtwitz, J. Petrasch, D. Trommer and A. Steinfeld, *Sol. Energy*, 2006, **80**, 1333–1337.
9 http://www.eia.gov/naturalgas/.
10 K. Aasberg-Petersen, T. S. Christensen, C. S. Nielsen and I. Dybkjær, *Fuel Process. Technol.*, 2003, **83**, 253–261.
11 F. Joensen and J. R. Rostrup-Nielsen, *J. Power Sources*, 2002, **105**, 195–201.
12 T. V. Choudhary and V. R. Choudhary, *Angew. Chem., Int. Ed.*, 2008, **47**, 1828–1847.
13 P. Tang, Q. Zhu, Z. Wu and D. Ma, *Energy Environ. Sci.*, 2014, **7**, 2580–2591.
14 J. J. Spivey and G. Hutchingsb, *Chem. Soc. Rev.*, 2014, **43**, 792–803.
15 H. A. Dirksen and C. H. Riesz, *Ind. Eng. Chem. Res.*, 1953, **7**, 1562–1565.
16 W. W. Akers and D. P. Camp, *AIChE J.*, 1955, **1**, 471–475.
17 J. Xu and G. F. Froment, *AIChE J.*, 1989, **35**, 88–96.
18 J. Xu and G. F. Froment, *AIChE J.*, 1989, **35**, 97–103.
19 J.-W. Snoeck, G. F. Froment and M. Fowles, *J. Catal.*, 1997, **169**, 250–262.
20 K. Hou and R. Hughes, *Chem. Eng. J.*, 2001, **82**, 311–328.
21 J.-W. Snoeck, G. F. Froment and M. Fowles, *Ind. Eng. Chem. Res.*, 2002, **41**, 4252–4265.
22 M. C. Annesini, V. Piemonte and L. Turchetti, *Chem. Eng. Trans.*, 2007, **11**, 21–26.
23 D. S. A. Simakov and M. Sheintuch, *AIChE J.*, 2008, **54**, 2735–2750.
24 D. S. A. Simakov and M. Sheintuch, *AIChE J.*, 2011, **57**, 525–541.
25 F. Frusteri, L. Spadaro, F. Arena and A. Chuvilin, *Carbon*, 2002, **40**, 1063–1070.
26 S. D. Angeli, G. Monteleone, A. Giaconia and A. A. Lemonidou, *Int. J. Hydrogen Energy*, 2014, **39**, 1979–1997.
27 Y. Matsumura and T. Nakamori, *Appl. Catal., A*, 2004, **258**, 107–114.
28 J. R. Rostrup-Nielsen, *Catal. Today*, 1993, **18**, 305–324.
29 S. C. Tsang, J. B. Claridge and M. L. H. Green, *Catal. Today*, 1995, **23**, 3–15.
30 A. T. Ashcroft, A. K. Cheetham, M. L. H. Green and P. D. F. Vernon, *Nature*, 1991, **352**, 225–226.

31 J. R. Rostrup-Nielsen and J.-H. B. Hansen, *J. Catal.*, 1993, **144**, 38–49.
32 H. Wu, V. L. Parola, G. Pantaleo, F. Puleo, A. M. Venezia and L. F. Liotta, *Catalysts*, 2013, **3**, 563–583.
33 J. B. Claridge, A. P. E. York, A. J. Brungs, C. Marquez-Alvare, J. Sloan, S. C. Tsang and M. L. H. Green, *J. Catal.*, 1998, **180**, 85–100.
34 M. V. Iyer, L. P. Norcio, A. Punnoose, E. L. Kugler, M. S. Seehra and D. B. Dadyburjor, *Top. Catal.*, 2004, **29**, 197–200.
35 J. H. Bitter, K. Seshan and J. A. Lercher, *J. Catal.*, 1997, **171**, 279–286.
36 J. Wei and E. Iglesia, *J. Phys. Chem. B*, 2004, **108**, 4094–4103.
37 G. Jones, J. G. Jakobsen, S. S. Shim, J. Kleis, M. P. Andersson, J. Rossmeisl, F. Abild-Pedersen, T. Bligaard, S. Helveg, B. Hinnemann, J. R. Rostrup-Nielsen, I. Chorkendorff, J. Sehested and J. K. Nørskov, *J. Catal.*, 2008, **259**, 147–160.
38 Y. Chen, J. Cheng, P. Hu and H. Wang, *Surf. Sci.*, 2008, **602**, 2828–2834.
39 Y. Xu, A. C. Lausche, S. Wang, T. S. Khan, F. Abild-Pedersen, F. Studt, J. K. Nørskov and T. Bligaard, *New J. Phys.*, 2013, **15**, 125021.
40 J. Wei and E. Iglesia, *Phys. Chem. Chem. Phys.*, 2004, **6**, 3754–3759.
41 J. Wei and E. Iglesia, *J. Phys. Chem. B*, 2004, **108**, 7253–7262.
42 J. Wei and E. Iglesia, *Angew. Chem., Int. Ed.*, 2004, **43**, 3685–3688.
43 J. Wei and E. Iglesia, *J. Catal.*, 2004, **225**, 116–127.
44 J. Wei and E. Iglesia, *J. Catal.*, 2004, **224**, 370–383.
45 J. A. Keith, J. Anton, P. Kaghazchi and T. Jacob, in *Modeling and Simulation of Heterogeneous Catalytic Reactions: From the Molecular Process to the Technical System*, ed. O. Deutschmann, Wiley-VCH, Verlag GmbH & Co KGaA, Weinheim, Germany, 2012, pp. 1–37.
46 J. K. Nørskov, F. Abild-Pedersen, F. Studt and T. Bligaard, *Proc. Natl. Acad. Sci. U. S. A.*, 2011, **108**, 937–943.
47 R. M. Watwe, H. S. Bengaard, J. R. Rostrup-Nielsen, J. A. Dumesic and J. K. Nørskov, *J. Catal.*, 2000, **189**, 16–30.
48 F. Abild-Pedersen, O. Lytken, J. Engbæk, G. Nielsen, I. Chorkendorff and J. K. Nørskov, *Surf. Sci.*, 2005, **590**, 127–137.
49 J. Rostrup-Nielsen and J. K. Nørskov, *Top. Catal.*, 2006, **40**, 45–48.
50 T. Zhu, P. W. V. Grootel, I. A. W. Filot, S.-G. Sun, R. A. V. Santen and E. J. M. Hensen, *J. Catal.*, 2013, **297**, 227–235.
51 A. Vojvodic, *Catal. Lett.*, 2012, **142**, 728–735.
52 R. B. Levy and M. Boudart, *Science*, 1973, **181**, 547–549.
53 A. P. E. York, J. B. Claridge, A. J. Brungs, S. C. Tsang and M. L. H. Green, *Chem. Commun.*, 1997, 39–40.
54 M. V. Iyer, L. P. Norcio, E. L. Kugler and D. B. Dadyburjor, *Ind. Eng. Chem. Res.*, 2003, **42**, 2712–2721.
55 C.-J. Liu, J. Ye, J. Jiang and Y. Pan, *ChemCatChem*, 2011, **3**, 529–541.
56 M. H. Halabi, M. H. J. M. D. Croon, J. V. D. Schaaf, P. D. Cobden and J. C. Schouten, *Appl. Catal., A*, 2010, **389**, 68–79.
57 J. R. Rostrup-Nielsen, *Catal. Today*, 2000, **63**, 159–164.
58 M. Dan, M. Mihet, A. R. Biris, P. Marginean, V. Almasan, G. Borodi, F. Watanabe, A. S. Biris and M. D. Lazar, *React. Kinet., Mech. Catal.*, 2012, **105**, 173–193.
59 M. A. Nieva, M. M. Villaverde, A. Monzón, T. F. Garetto and A. J. Marchi, *Chem. Eng. J.*, 2014, **235**, 158–166.
60 K. Kusakabe, K.-I. Sotowa, T. Eda and Y. Iwamoto, *Fuel Process. Technol.*, 2004, **86**, 319–326.
61 J. Xu, C. M. Y. Yeung, J. Ni, F. Meunier, N. Acerbi, M. Fowles and S. C. Tsang, *Appl. Catal.*, 2008, **345**, 119–127.
62 J. H. Bitter, K. Seshan and J. A. Lercher, *J. Catal.*, 1998, **176**, 93–101.
63 A. M. O'Connor, Y. Schuurman, J. R. H. Ross and C. Mirodatos, *Catal. Today*, 2006, **115**, 191–198.
64 J. G. Jakobsen, M. Jakobsen, I. Chorkendorff and J. Sehested, *Catal. Lett.*, 2010, **140**, 90–97.
65 J. G. Jakobsen, T. L. Jørgensen, I. Chorkendorff and J. Sehested, *Appl. Catal., A*, 2010, **377**, 158–166.
66 R. B. Duarte, O. V. Safonova, F. Krumeich, M. Makosch and J. A. V. Bokhoven, *ACS Catal.*, 2013, **3**, 1956–1964.
67 J. Múnera, S. Irusta, L. Cornaglia and E. Lombardo, *Appl. Catal., A*, 2003, **245**, 383–395.
68 C. Carrara, J. Munera, E. A. Lombardo and L. M. Cornaglia, *Top. Catal.*, 2008, **51**, 98–106.
69 P. Ferreira-Aparicio, C. Marquez-Alvarez, I. Rodrıguez-Ramos, Y. Schuurman, A. Guerrero-Ruiz and C. Mirodatos, *J. Catal.*, 1999, **184**, 202–212.
70 A. Al-Ubaid and E. E. Wolf, *Appl. Catal.*, 1987, **34**, 119–134.
71 P. Frontera, A. Aloise, A. Macario, F. Crea, P. L. Antonucci, G. Giordano and J. B. Nagy, *Res. Chem. Intermed.*, 2011, **37**, 267–279.
72 P. Frontera, A. Aloise, A. Macario, P. L. Antonucci, F. Crea, G. Giordano and J. B. Nagy, *Top. Catal.*, 2010, **53**, 265–272.
73 U. L. P. Portugal Jr., C. M. P. Marques, E. C. C. Araujo, E. V. Morales, M. V. Giotto and J. M. C. Bueno, *Appl. Catal., A*, 2000, **193**, 173–183.
74 S. M. Gheno, S. Damyanova, B. A. Riguetto, C. M. P. Marques, C. A. P. Leite and J. M. C. Buenoa, *J. Mol. Catal. A: Chem.*, 2003, **198**, 263–275.
75 Y. Schuurman, C. Mirodatos, P. Ferreira-Aparicio, I. Rodrıguez-Ramos and A. Guerrero-Ruiz, *Catal. Lett.*, 2000, **66**, 33–37.
76 L. C. S. Kahle, T. Roussière, L. Maier, K. H. Delgado, G. Wasserschaff, S. A. Schunk and O. Deutschmann, *Ind. Eng. Chem. Res.*, 2013, **52**, 11920–11930.
77 Y. Sekine, M. Haraguchi, M. Matsukata and E. Kikuchi, *Catal. Today*, 2011, **171**, 116–125.
78 D. A. J. M. Ligthart, R. A. V. Santen and E. J. M. Hensen, *J. Catal.*, 2011, **280**, 206–220.
79 V. M. Shinde and G. Madras, *Int. J. Hydrogen Energy*, 2013, **38**, 13961–13973.
80 B. T. Schadel, M. Duisberg and O. Deutschmann, *Catal. Today*, 2009, **142**, 42–51.

81 U.-E.-S. Amjad, A. Vita, C. Galletti, L. Pino and S. Specchia, *Ind. Eng. Chem. Res.*, 2013, **52**, 15428–15436.
82 A. Berman, R. K. Karn and M. Epstein, *Appl. Catal., A*, 2005, **282**, 73–83.
83 J. R. Rostrup-Nielsen, *J. Catal.*, 1973, **31**, 173–199.
84 D. Qin and J. Lapszewicz, *Catal. Today*, 1994, **21**, 551–560.
85 D. S. A. Simakov, H. Y. Luo and Y. Román-Leshkov, Ultra-low loading Ru/γ-Al2O3: a highly active and stable catalyst for low temperature solar thermal reforming of methane, *Appl. Catal., B*, 2015, DOI: 10.1016/j.apcatb.2015.01.011.
86 Y. Xu, C. Fan, Y.-A. Zhu, P. Li, X.-G. Zhou, D. Chen and W.-K. Yuan, *Catal. Today*, 2012, **186**, 54–62.
87 N. V. Parizotto, D. Zanchet, K. O. Rocha, C. M. P. Marques and J. M. C. Bueno, *Appl. Catal., A*, 2009, **366**, 122–129.
88 C. Crisafulli, S. Scire, R. Maggiore, S. Minico and S. Galvagno, *Catal. Lett.*, 1999, **59**, 21–26.
89 M. M. B. Quiroga and A. E. C. Luna, *Ind. Eng. Chem. Res.*, 2007, **46**, 5265–5270.
90 M. García-Diéguez, I. S. Pieta, M. C. Herrera, M. A. Larrubia and L. J. Alemany, *J. Catal.*, 2010, **270**, 136–145.
91 L. Guczi, G. Stefler, O. Geszti, I. Sajo, Z. Paszti, A. Tompos and Z. Schay, *Appl. Catal., A*, 2010, **375**, 236–246.
92 S. Damyanova, B. Pawelec, K. Arishtirova, J. L. G. Fierro, C. Sener and T. Dogu, *Appl. Catal., B*, 2009, **92**, 250–261.
93 M. Nowosielska, W. K. Jozwiak and J. Rynkowski, *Catal. Lett.*, 2009, **128**, 83–93.
94 J.-S. Choi, K.-I. Moon, Y. G. Kim, J. S. Lee, C.-H. Kim and D. L. Trimm, *Catal. Lett.*, 1998, **52**, 43–47.
95 H. Liu, C. Guan, X. Li, L. Cheng, J. Zhao, N. Xue and W. Ding, *ChemCatChem*, 2013, **5**, 3904–3909.
96 J. Zhang, H. Wang and A. K. Dalai, *J. Catal.*, 2007, **249**, 300–310.
97 M. Khzouz, J. Wood, B. Pollet and W. Bujalski, *Int. J. Hydrogen Energy*, 2013, **38**, 1664–1675.
98 J. Lemaitre, B. Vidick and B. Delmon, *J. Catal.*, 1986, **99**, 415–427.
99 J. S. Lee, S. T. Oyama and M. Boudart, *J. Catal.*, 1987, **106**, 125–133.
100 J. S. Lee, L. Volpe, F. H. Ribeiro and M. Boudart, *J. Catal.*, 1988, **112**, 44–53.
101 A. J. Brungs, A. P. E. York and M. L. H. Green, *Catal. Lett.*, 1999, **57**, 65–69.
102 H. Shao, E. L. Kugler, W. Ma and D. B. Dadyburjor, *Ind. Eng. Chem. Res.*, 2005, **44**, 4914–4921.
103 J. R. H. Ross, *Catal. Today*, 2005, **100**, 151–158.
104 A. J. Brungs, A. P. E. York, J. B. Claridge, C. Marquez-Alvarez and M. L. H. Green, *Catal. Lett.*, 2000, **70**, 117–122.
105 C. Agrafiotis, H. von Storch, M. Roeb and C. Sattler, *Renewable Sustainable Energy Rev.*, 2014, **29**, 656–682.
106 A. Giaconia, M. D. Falco, G. Caputo, R. Grena, P. Tarquini and L. Marrelli, *AIChE J.*, 2008, **54**, 1932–1944.
107 M. D. Falco, A. Giaconia, L. Marrelli, P. Tarquini, R. Grena and G. Caputo, *Int. J. Hydrogen Energy*, 2009, **34**, 98–109.
108 M. D. Falco and V. Piemonte, *Int. J. Hydrogen Energy*, 2011, **36**, 7759–7762.
109 A. Giaconia, L. Turchetti, G. Monteleone, B. Morico, G. Iaquaniello, K. Shabtai, M. Sheintuch, D. Boettge, J. Adler, V. Palma, S. Voutetakis, A. Lemonidou, M. C. Annesini, M. D. Exter and H. Balzer, *Chem. Eng. Trans.*, 2013, **35**, 433–438.
110 J. T. Richardson and S. A. Paripatyadar, *Appl. Catal.*, 1990, **61**, 293–309.
111 S. A. Paripatyadar and J. T. Richardson, *Sol. Energy*, 1988, **41**, 475–485.
112 J. T. Richardson, S. A. Paripatyadar and J. C. Shen, *AIChE J.*, 1988, **34**, 743–752.
113 R. B. Diver, J. D. Fish, R. Levitan, M. Levy, E. Meirovitch, H. Rosin, S. A. Paripatyadar and J. T. Richardson, *Sol. Energy*, 1992, **48**, 21–30.
114 J. H. McCrary and G. E. McCrary, *Sol. Energy*, 1982, **29**, 141–151.
115 G. D. Maria, L. D'Alessio, E. Coffari, M. Paolucci and C. A. Tiberio, *Sol. Energy*, 1985, **35**, 409–416.
116 G. D. Maria, C. A. Tiberio, L. D'Alessio, M. Piccirilli, E. Coffari and M. Paolucci, *Energy*, 1986, **11**, 805–810.
117 M. Levy, H. Rosin and R. Levitan, *J. Sol. Energy Eng.*, 1989, **111**, 96–97.
118 J. R. E. Hogan, R. D. Skocypec, R. B. Diver and J. D. Fish, *Chem. Eng. Sci.*, 1990, **45**, 2751–2758.
119 R. Buck, J. F. Muir, R. E. Hogan and R. D. Skocypec, *Sol. Energy Mater.*, 1991, **24**, 449–463.
120 M. Levy, R. Rubin, H. Rosin and R. Levitan, *Energy*, 1992, **17**, 749–756.
121 J. F. Muir, J. Roy, E. Hogan, R. D. Skocypec and R. Buck, *Sol. Energy*, 1994, **52**, 467–477.
122 R. D. Skocypec, J. Roy, E. Hogan and J. F. Muir, *Sol. Energy*, 1994, **52**, 479–490.
123 V. I. Anikeev, A. S. Bobrin, J. Ortner, S. Schmidt, K.-H. Funken and N. A. Kuzin, *Sol. Energy*, 1998, **63**, 97–104.
124 A. Worner and R. Tamme, *Catal. Today*, 1998, **46**, 165–174.
125 R. Tamme, R. Buck, M. Epstein, U. Fisher and C. Sugarmen, *J. Sol. Energy Eng.*, 2001, **123**, 160–163.
126 T. Kodama, A. Kiyama and K.-I. Shimizu, *Energy Fuels*, 2003, **17**, 13–17.
127 J. K. Dahl, A. W. Weimer, A. Lewandowski, C. Bingham, F. Bruetsch and A. Steinfeld, *Ind. Eng. Chem. Res.*, 2004, **43**, 5489–5495.
128 T. Kodama, A. Kiyama, T. Moriyama and O. Mizuno, *J. Sol. Energy Eng.*, 2004, **126**, 808–811.
129 A. Berman, R. K. Karn and M. Epstein, *Green Chem.*, 2007, **9**, 626–631.
130 J. Petrasch and A. Steinfeld, *Chem. Eng. Sci.*, 2007, **62**, 4214–4228.
131 R. Rubin and J. Karni, *J. Sol. Energy Eng.*, 2011, **133**, 021008.
132 H. B. Do, J. T. Jang and G. Y. Han, *J. Sol. Energy Eng.*, 2012, **134**, 041013.
133 T. Kodama, N. Gokon, S.-I. Inuta and S. Yamashita, *J. Sol. Energy Eng.*, 2009, **131**, 041013.
134 T. Kodama, T. Koyanagi, T. Shimizu and Y. Kitayama, *Energy Fuels*, 2001, **15**, 60–65.
135 N. Gokon, Y. Oku, H. Kaneko and Y. Tamaura, *Sol. Energy*, 2002, **72**, 243–250.

